RESEARCH ARTICLE

Impact Time and Angle Control Guidance: Cooperative Guidability and Gain Synthesis

Lanhao Zhao[1] **and Guangxin Guo**[2,*]

[1] College of Information Science and Technology, Beijing University of Technology, Beijing 100124, China
[2] School of Systems Science and Engineering, Sun Yat-sen University, Guangzhou 510275, China

Abstract

Cooperative guidance of multi-missile salvo systems has emerged as a cornerstone technology in modern aerospace defense and precision strike operations. Impact Time and Angle Control Guidance (ITACG) schemes frequently rely on piecewise stage switching to bypass terminal singularities and brute-force post-hoc tuning that cannot certify gain feasibility under actuator saturation prior to launch. To overcome these limitations, this paper establishes a fully coupled, singularity-free guidance architecture and a pre-launch theoretical framework termed Cooperative Guidability. First, embedding relative distance into a logarithmic Barrier Lyapunov Function (BLF) virtual control law algebraically cancels inverse-range singularities and confines the lead angle, while a smooth threshold mapping eliminates dead-zone chattering. Second, employing Vector Lyapunov Functions (VLF) and M-matrix theory to decouple spatiotemporal perturbations, we reveal a two-sided hyperbolic-linear gain squeeze mechanism and derive closed-form optimal gains. Finally, explicit necessary and sufficient criteria, governed by a dimensionless guidability index and network connectivity thresholds, are established across ideal, uncertain, and maneuvering-target scenarios, yielding two graphical verification tools confirmed by numerical simulations.

Keywords: cooperative guidance, cooperative guidability, Vector Lyapunov Function (VLF), Barrier Lyapunov Function (BLF), M-matrix, terminal singularity, actuator saturation.

1 Introduction

Cooperative guidance of multi-missile salvo systems has emerged as a cornerstone technology in modern aerospace defense and precision strike operations to neutralize heavily defended high-value targets [1–6]. By orchestrating multiple missiles to arrive at a designated target simultaneously from pre-assigned spatial azimuth angles, a salvo system not only saturates the defense of advanced close-in weapon systems (CIWS)[7], but also, through prescribed terminal impact angles under seeker field-of-view limits, attacks the target's structural weak spots to maximize warhead lethality [8, 9]. Within the aerospace guidance community, this multi-agent

Submitted: 17 September 2026
Revised: 30 October 2026
Accepted: 01 November 2026
Published: 23 November 2026

Vol. 1, **No.** 4, 2026.
10.62762/AEC.2026.805686

***Corresponding author:**
✉Guangxin Guo
xinpx1457@163.com

Citation
Zhao, L., & Guo, G. (2026). Impact Time and Angle Control Guidance: Cooperative Guidability and Gain Synthesis. *Aerospace Engineering Communications*, 1(4), 137–153.

© 2026 by the Authors. Published by Institute of Central Computation and Knowledge. This is an open access article under the CC BY license (https://creativecommons.org/licenses/by/4.0/).

spatiotemporal coordination challenge is formally cast as the Impact Time and Angle Control Guidance (ITACG) problem [10–12]. Unlike standalone trajectory tracking, the ITACG paradigm requires distributed time-to-go synchronization over an inter-missile communication network while strictly respecting individual aerodynamic overload and seeker field-of-view (FOV) constraints, thereby motivating intensive research into advanced cooperative guidance architectures.

To address the multi-constraint nature of the ITACG problem, contemporary research has developed a diverse spectrum of mainstream algorithmic frameworks ranging from analytical nonlinear control to data-driven reinforcement learning [13–15]. Broadly speaking, existing analytical solutions predominantly rely on optimal control theory[16], sliding mode control (SMC)[17], finite- or fixed-time distributed consensus protocols[18–21], and Barrier Lyapunov Function (BLF) techniques for constraint handling[22] to drive inter-missile impact-time disagreements and line-of-sight (LOS) angle errors to zero [13, 14, 23], where finite-time stabilization theory [23] guarantees convergence within a prescribed flight horizon. Concurrently, computational intelligence methods, such as Multi-Agent Proximal Policy Optimization (MAPPO)[15], have been increasingly explored to learn cooperative maneuvering policies directly from high-dimensional engagement environments. While these mainstream methodologies demonstrate promising kinematic accuracy under nominal settings, their practical deployment is severely hindered when confronted with the intrinsic singularities and strong nonlinear cross-couplings of terminal missile-target kinematics.

Specifically, the inherent terminal and internal singularities embedded in relative engagement kinematics frequently force existing guidance laws into piecewise two-stage switching strategies that compromise flight stability and continuous controllability [2, 14]. Because the LOS angular rate equation inherently contains the relative distance R_i in its denominator, the $1/R_i$ factor embedded in conventional backstepping or proportional feedback laws diverges to infinity as the missile approaches the target ($R_i \to 0$). To bypass this terminal singularity, mainstream schemes commonly adopt a "two-stage" decoupling strategy—coordinating impact time during the midcourse phase and hard-switching to impact-angle tracking or proportional navigation guidance (PNG) during the terminal phase [2, 14]. However, such discontinuous stage switching inevitably triggers abrupt lateral acceleration jumps that jeopardize the stability margin of the onboard autopilot, while forfeiting terminal closed-loop temporal correction against late-stage perturbations. Moreover, even if a single-stage coupled law is retained, executing large midcourse lead-angle maneuvers ($\theta_{Mi} \to \pm\pi/2$) to dissipate excess time-to-go drives $\cos\theta_{Mi} \to 0$ in the control denominator, inducing an internal singularity that calls for explicit lead-angle confinement, as provided by BLF-based constraint handling [22]; conversely, when θ_{Mi} traverses zero degrees mid-flight, the nominal temporal control gain $G_{ti} \to 0$ causes an instantaneous loss of temporal controllability (the dead-zone effect). Overcoming these dual singularities without stage switching demands a globally smooth, fully coupled control protocol, which in turn exposes a formidable theoretical challenge in analyzing bidirectional spatiotemporal cross-couplings.

Capturing the bidirectional energy exchange within a singularity-free, fully coupled guidance architecture necessitates transcending traditional scalar Lyapunov analysis via the Vector Lyapunov Function (VLF) methodology [24–26]. In a fully coupled salvo framework, the spatial angle tracking command u_{qi} continuously alters trajectory curvature and injects strong interconnected perturbations into the distributed temporal consensus network; reciprocally, the temporal coordination command u_{ti} directly perturbs the inner-loop lead-angle tracking dynamics. Traditional single scalar Lyapunov functions aggregate these heterogeneous state errors into a single weighted sum, which obscures the structural interaction between local nonlinear kinematics and the communication graph Laplacian topology [27], often forcing stability proofs to rely on fragile time-scale separation assumptions. By contrast, the VLF framework [25, 26] preserves the topological integrity of large-scale interconnected systems by constructing a multi-dimensional energy vector governed by a comparison Z-matrix. Through M-matrix stability theory, VLF analysis not only provides a rigorous algebraic mechanism to decouple bidirectional spatiotemporal perturbations, but also establishes explicit quantitative links between controller gains, coupling intensities, and network algebraic connectivity, paving the way for a deeper inquiry into physical gain feasibility.

Crucially, even with rigorous stability tools, existing

paradigms remain trapped in a brute-force post-hoc verification workflow that lacks an *a priori* theoretical criterion—termed *Cooperative Guidability*—to certify whether a feasible control solution physically exists prior to launch. Predominant synthesis approaches—whether based on empirical gain tuning, numerical trajectory optimization, or brute-force reinforcement learning training—operate on the blind premise that a valid controller parameter set is usable only after it has been explicitly solved or tuned via exhaustive trial-and-error simulations. This brute-force paradigm fails to answer a far more fundamental systems-science question: *Given a specific initial launch geometry, communication topology connectivity, maximum physical missile overload $a_{\max}$, and a prescribed protocol structure, does there mathematically exist a set of controller gain parameters capable of achieving cooperative interception within the finite flight horizon T_f?* If harsh initial conditions or weak network connectivity render the parameter feasibility space empty—meaning the minimum theoretical gains required to suppress spatiotemporal cross-couplings inevitably breach the physical actuator saturation limit $a_{\max}$—any online parameter tuning, numerical optimization, or brute-force policy training is destined to fail. Formulating Cooperative Guidability fundamentally overcomes this defect, shifting multi-missile fire control from blind numerical trial-and-error to deterministic pre-launch feasibility certification and analytical gain synthesis.

Motivated by the aforementioned challenges, this paper establishes a unified theoretical framework of ***Cooperative Guidability*** and closed-form optimal gain synthesis for fully coupled, singularity-free multi-missile salvo systems. By integrating distance-embedded Barrier Lyapunov Function (BLF) design with VLF comparison theory and shifted M-matrix analysis, this work bridges the gap between continuous protocol synthesis and *a priori* mission verification. The primary contributions of this work are threefold:

- **Fully Coupled Smooth Protocol with Algebraic Dual-Singularity Elimination:** By synthesizing the backstepping technique with a logarithmic Barrier Lyapunov Function (BLF), the relative distance factor R_i is explicitly embedded inside the hyperbolic tangent argument of the virtual control law. Consequently, the R_i multiplier generated during virtual control differentiation algebraically cancels the $1/R_i$ denominator in the LOS rate dynamics, eradicating terminal singularity without small-angle approximations. Simultaneously, the BLF strictly confines the inner-loop state to prevent the internal singularity ($\cos\theta_{Mi} = 0$), while a globally smooth C^∞ threshold mapping $\bar{G}_{ti}$ absorbs the zero-crossing dead-zone effect without chattering.

- **Rigorous Mathematical Definition of Cooperative Guidability and the Two-Sided Gain Squeeze Mechanism:** Cooperative Guidability under a prescribed protocol structure is formulated as the non-emptiness problem of the intersection between the finite-horizon theoretical convergence gain set $\mathcal{K}_{\text{theory}}(\sigma_0)$ and the physical overload admissible set $\mathcal{K}_{\text{physical}}(a_{\max})$. Leveraging VLF and shifted M-matrix theory, we rigorously prove that spatial and temporal control gains are subjected to a geometric "two-sided squeeze" bounded below by a stability hyperbola and above by an actuator saturation line.

- **Explicit Necessary and Sufficient Criteria and Closed-Form Optimal Gain Synthesis Across Three Scenarios:** We derive the dimensionless Cooperative Guidability Index (Ξ_{CG}) and explicit temporal consensus synchronization conditions across ideal kinematics, internal parametric uncertainties, and external target maneuvers, proving that $\Xi_{\text{CG}} \leq 1$ coupled with minimum algebraic connectivity thresholds is both necessary and sufficient for a non-empty parameter feasibility space under the VLF envelope. Furthermore, using the AM-GM inequality, we obtain the closed-form analytical solution for the globally unique optimal gain saddle point (K_S^*, K_T^*) that minimizes peak overload demand, accompanied by two graphical rapid-verification tools for pre-launch fire-control assessment.

2 Multi-Missile System Modeling and Control Protocol Formulation

2.1 Graph Theory Preliminaries and Algebraic Connectivity

Consider a cooperative salvo group of n missiles exchanging time-to-go information over an undirected connected communication graph $\mathcal{G} = (\mathcal{V}, \mathcal{E}, \mathcal{A})$, where $\mathcal{V} = \{1, 2, \ldots, n\}$ denotes the node set, $\mathcal{E} \subseteq \mathcal{V} \times \mathcal{V}$ denotes the edge set, and $\mathcal{A} = [a_{ij}] \in \mathbb{R}^{n\times n}$ represents the weighted adjacency matrix. If a bidirectional communication link exists between missile i and

missile j, then $a_{ij} = a_{ji} > 0$; otherwise, $a_{ij} = 0$ (with self-loop weights $a_{ii} = 0$). The graph Laplacian matrix is defined as $L = \mathcal{D} - \mathcal{A}$, where $\mathcal{D} = \text{diag}\{d_1, \ldots, d_n\}$ is the degree matrix with $d_i = \sum_{j=1}^{n} a_{ij}$.

Lemma 1 (Algebraic Connectivity Properties [27]). *If the undirected graph $\mathcal{G}$ is connected, the Laplacian matrix L is real, symmetric, and positive semi-definite ($L = L^T \geq 0$). Zero is a simple eigenvalue of L with the associated eigenvector $\mathbf{1}_n = [1, \ldots, 1]^T$. Ordering the eigenvalues in ascending order as $0 = \lambda_1(L) < \lambda_2(L) \leq \cdots \leq \lambda_n(L)$, the smallest non-zero eigenvalue $\lambda_2(L) > 0$ is defined as the **algebraic connectivity** of $\mathcal{G}$. For any state vector $\mathbf{x} \in \mathbb{R}^n$ orthogonal to $\mathbf{1}_n$ (i.e., $\mathbf{1}_n^T \mathbf{x} = 0$), the Courant-Fischer Rayleigh quotient inequalities strictly hold:*

$$\begin{aligned} \lambda_2(L)\|\mathbf{x}\|_2^2 \leq \mathbf{x}^T L \mathbf{x} \leq \lambda_n(L)\|\mathbf{x}\|_2^2 \\ \lambda_2^2(L)\|\mathbf{x}\|_2^2 \leq \mathbf{x}^T L^2 \mathbf{x} \leq \lambda_n^2(L)\|\mathbf{x}\|_2^2 \end{aligned} \tag{1}$$

2.2 Relative Kinematics and Fully Coupled Time-to-Go Dynamics

Consider a planar engagement scenario where n missiles intercept a stationary or maneuvering target located at the origin of the inertial coordinate system X-O-Y. For the i-th missile ($i \in \mathcal{V}$), let V_{Mi} denote its constant velocity, R_i the relative missile-target distance, q_i the line-of-sight (LOS) angle, and ψ_i the flight path angle. Define the missile lead angle (heading error) as $\theta_{Mi} \triangleq \psi_i - q_i$. Incorporating target maneuver velocity components and unmodeled perturbations, the nonlinear planar relative kinematics are governed by:

$$\begin{cases} \dot{R}_i = -V_{Mi}\cos\theta_{Mi} + v_{Ti\parallel}(t) \\ \dot{q}_i = -\dfrac{V_{Mi}}{R_i}\sin\theta_{Mi} + d_{qi}(t) \\ \dot{\theta}_{Mi} = \dfrac{a_{Mi}}{V_{Mi}} - \dot{q}_i = \dfrac{a_{Mi}}{V_{Mi}} + \dfrac{V_{Mi}}{R_i}\sin\theta_{Mi} - d_{qi}(t) \end{cases} \tag{2}$$

where a_{Mi} is the lateral acceleration command of missile i, physically constrained by aerodynamic saturation $|a_{Mi}(t)| \leq a_{\max}$; $v_{Ti\parallel}(t)$ and $v_{Ti\perp}(t)$ represent the projections of the target velocity along and perpendicular to the LOS, respectively; and $d_{qi}(t) \triangleq \frac{v_{Ti\perp}(t)}{R_i}$ denotes the external disturbance injected into the LOS angular rate channel by target maneuvers, where the target lateral acceleration satisfies $|a_T(t)| \leq a_{T\max}$.

Without invoking small-angle linearization, the estimated time-to-go $t_{go,i}$ of the i-th missile is formulated via a second-order nonlinear Taylor series expansion:

$$t_{go,i} = \frac{R_i}{V_{Mi}}\left(1 + \frac{\theta_{Mi}^2}{2}\right) + \mathcal{O}(\theta_{Mi}^3) \tag{3}$$

Differentiating (3) with respect to time along the kinematic trajectories (2) and expanding all terms explicitly yields:

$$\begin{aligned} \dot{t}_{go,i} &= \frac{\dot{R}_i}{V_{Mi}}\left(1 + \frac{\theta_{Mi}^2}{2}\right) + \frac{R_i\theta_{Mi}}{V_{Mi}}\dot{\theta}_{Mi} + \frac{d}{dt}\mathcal{O}(\theta_{Mi}^3) \\ &= -\cos\theta_{Mi}\left(1 + \frac{\theta_{Mi}^2}{2}\right) + \frac{R_i\theta_{Mi}}{V_{Mi}}\left(\frac{a_{Mi}}{V_{Mi}} + \frac{V_{Mi}\sin\theta_{Mi}}{R_i}\right) \\ &\quad + \frac{v_{Ti\parallel}(t)}{V_{Mi}}\left(1 + \frac{\theta_{Mi}^2}{2}\right) - \frac{R_i\theta_{Mi}}{V_{Mi}}d_{qi}(t) + \frac{d}{dt}\mathcal{O}(\theta_{Mi}^3) \\ &= -1 + \frac{R_i\theta_{Mi}}{V_{Mi}^2}a_{Mi} \\ &\quad + \underbrace{\left[1 - \cos\theta_{Mi}\left(1 + \frac{\theta_{Mi}^2}{2}\right) + \theta_{Mi}\sin\theta_{Mi} + \frac{d}{dt}\mathcal{O}(\theta_{Mi}^3)\right]}_{\text{High-order truncation \& internal parametric uncertainty } \Delta_i(t)} \\ &\quad + d_{ti}(t) \end{aligned} \tag{4}$$

Defining the nominal temporal control gain as:

$$G_{ti}(\mathbf{x}_i) \triangleq +\frac{R_i\theta_{Mi}}{V_{Mi}^2} \tag{5}$$

the time-to-go dynamics (4) can be compactly expressed in the perturbed control-affine form:

$$\dot{t}_{go,i} = -1 + G_{ti}(\mathbf{x}_i)a_{Mi} + \Delta_i(t) + d_{ti}(t) \tag{6}$$

where $\Delta_i(t)$ encapsulates the nonlinear residual (of order $\mathcal{O}(\theta_{Mi}^2)$, dominated by $\theta_{Mi}\sin\theta_{Mi}$, plus the Taylor truncation terms) and internal aerodynamic parameter deviations, while $d_{ti}(t) \triangleq \frac{v_{Ti\parallel}(t)}{V_{Mi}}(1 + \frac{\theta_{Mi}^2}{2}) - \frac{R_i\theta_{Mi}}{V_{Mi}}d_{qi}(t)$ represents the external temporal disturbance induced by target maneuvers. Note from (5) that when $\theta_{Mi} > 0$, applying a positive lateral acceleration $a_{Mi} > 0$ increases the trajectory curvature and lengthens the flight path, thereby increasing $t_{go,i}$ ($\frac{\partial \dot{t}_{go,i}}{\partial a_{Mi}} = G_{ti} > 0$).

2.3 Fully Coupled Continuous Control Protocol with Dual-Singularity Elimination

To simultaneously achieve spatial impact-angle tracking ($q_i \to q_{id}$) and temporal impact-time consensus ($t_{go,i} \to t_{go,j}$), the lateral acceleration command is synthesized via a fully coupled linear superposition structure:

$$a_{Mi} = u_{qi} + u_{ti} \tag{7}$$

where u_{qi} denotes the spatial angle tracking control law and u_{ti} denotes the distributed temporal consensus control law.

2.3.1 Spatial Angle Control Law u_{qi} via Distance-Embedded Backstepping and BLF

Define the outer-loop LOS angle tracking error as:

$$z_{1i} \triangleq q_i - q_{id} \tag{8}$$

whose time derivative along (2) is $\dot{z}_{1i} = -\frac{V_{Mi}}{R_i}\sin\theta_{Mi} + d_{qi}(t)$. In conventional backstepping designs, choosing a standard proportional virtual control $\alpha_i = k_1 z_{1i}$ forces its time derivative $\dot{\alpha}_i = k_1\dot{z}_{1i} = -\frac{k_1 V_{Mi}}{R_i}\sin\theta_{Mi}$ to diverge to infinity as $R_i \to 0$.

To eradicate this terminal singularity at its root, we treat $\sin\theta_{Mi}$ as the virtual control input for the outer loop and explicitly embed the relative distance R_i inside the hyperbolic tangent function to construct a strictly bounded virtual control law:

$$\alpha_i(t) \triangleq \lambda_0 \tanh\left(\bar{k}_1 K_S R_i z_{1i}\right) \tag{9}$$

where $K_S > 0$ is the spatial master gain parameter to be synthesized, $\bar{k}_1 > 0$ is a baseline scaling constant, and $\lambda_0 \in (0, \sin\theta_{\max})$ is the virtual control saturation margin, with $\theta_{\max} \in (0, \pi/2)$ denoting the maximum permissible seeker field-of-view (FOV) / lead angle limit.

Define the inner-loop lead-angle tracking error as:

$$z_{2i} \triangleq \sin\theta_{Mi} - \alpha_i \tag{10}$$

Substituting (10) into the nominal $\dot{z}_{1i}$ equation and differentiating $\alpha_i(t)$ with respect to time along the nominal kinematics (letting $s_i \triangleq \bar{k}_1 K_S R_i z_{1i}$) yields the exact chain-rule expansion:

$$\begin{aligned}\dot{\alpha}_i &= \lambda_0 \mathrm{sech}^2(s_i)\cdot \bar{k}_1 K_S\left(\dot{R}_i z_{1i} + R_i \dot{z}_{1i}\right)\\ &= \lambda_0 \bar{k}_1 K_S \mathrm{sech}^2\left(\bar{k}_1 K_S R_i z_{1i}\right)\\ &\quad\times\left[\left(-V_{Mi}\cos\theta_{Mi}\right) z_{1i} + R_i\left(-\frac{V_{Mi}}{R_i}\sin\theta_{Mi}\right)\right]\\ &= -\lambda_0 \bar{k}_1 K_S V_{Mi}\mathrm{sech}^2\left(\bar{k}_1 K_S R_i z_{1i}\right)\left(z_{1i}\cos\theta_{Mi} + \sin\theta_{Mi}\right)\end{aligned} \tag{11}$$

Inspecting (11) reveals a critical algebraic property: the R_i multiplier generated by the product rule exactly cancels the $1/R_i$ denominator in $\dot{z}_{1i}$. Consequently, throughout the entire engagement envelope right up to impact ($R_i \to 0$), the virtual control derivative $\dot{\alpha}_i$ remains strictly bounded, completely eliminating the "explosion of complexity" and terminal singularity in backstepping.

To strictly guarantee that the lead angle satisfies $|\theta_{Mi}(t)| < \theta_{\max} < \pi/2$ for all $t \geq 0$ (thereby ensuring $\cos\theta_{Mi} > \cos\theta_{\max} > 0$ and structurally preventing internal singularity), we construct a logarithmic Barrier Lyapunov Function (BLF) for each missile's spatial subsystem:

$$V_{1i}(z_{1i}, z_{2i}) \triangleq \frac{1}{2}z_{1i}^2 + \frac{1}{2}\ln\left(\frac{k_b^2}{k_b^2 - z_{2i}^2}\right) \tag{12}$$

where $k_b \triangleq \sin\theta_{\max} - \lambda_0 > 0$ defines the safe barrier boundary for the inner-loop error z_{2i}.

Based on the BLF structure (12), the spatial angle tracking control law u_{qi} is synthesized as:

$$\begin{aligned}u_{qi} = \frac{V_{Mi}}{\cos\theta_{Mi}}\Bigg[&-\bar{k}_2 K_S z_{2i} + \dot{\alpha}_i - \frac{V_{Mi}\sin\theta_{Mi}\cos\theta_{Mi}}{R_i}\\ &+\left(k_b^2 - z_{2i}^2\right)\frac{V_{Mi}}{R_i}z_{1i}\Bigg]\end{aligned} \tag{13}$$

where $\bar{k}_2 > 0$ is the baseline inner-loop scaling constant.

Remark 1 (Boundedness at Terminal Blind-Zone Handover)**.** *Although the last two kinematics-compensation terms inside the bracket of (13) contain R_i in the denominator, physical interceptors trigger warhead detonation or blind-zone handover at a small non-zero terminal radius $R_{\min}$ (e.g., 0.1–8 m). Provided the spatial errors (z_{1i}, z_{2i}) decay at an exponential rate σ_0 faster than the geometric LOS divergence rate such that $|z_{1i}(t)| = \mathcal{O}(R_i)$ and $|\sin\theta_{Mi}(t)| = \mathcal{O}(R_i)$, the ratios $\frac{\sin\theta_{Mi}}{R_i}$ and $\frac{z_{1i}}{R_i}$ remain strictly bounded. Furthermore, since the BLF enforces $|z_{2i}(t)| < k_b$, the triangle inequality guarantees $|\sin\theta_{Mi}| \leq |z_{2i}| + |\alpha_i| < k_b + \lambda_0 = \sin\theta_{\max} < 1$, rendering the division by $\cos\theta_{Mi} \geq \cos\theta_{\max} > 0$ globally non-singular.*

2.3.2 Temporal Consensus Control Law u_{ti} with Smooth Dead-Zone Crossing

Define the local time-to-go consensus error for the i-th missile as:

$$e_{ti} \triangleq \sum_{j=1}^{n} a_{ij}\left(t_{go,i} - t_{go,j}\right) \tag{14}$$

which can be stacked into the global vector form $\mathbf{e}_T = [e_{t1}, \ldots, e_{tn}]^T = L\mathbf{t}_{go}$. In standard coupled ITACG laws, whenever θ_{Mi} crosses zero midcourse ($\theta_{Mi} = 0$), the nominal temporal gain $G_{ti} = +\frac{R_i\theta_{Mi}}{V_{Mi}^2}$ vanishes, causing a loss of temporal controllability. Inverting G_{ti} directly causes control divergence, whereas using discontinuous $\mathrm{sgn}(\theta_{Mi})$ switching induces violent

chattering. To ensure smooth dead-zone traversal while preserving the correct feedback polarity, we construct a globally C^∞ smooth non-singular temporal gain mapping $\bar{G}_{ti}(\mathbf{x}_i)$:

$$\bar{G}_{ti}(\mathbf{x}_i) \triangleq +\frac{R_i}{V_{Mi}^2}\sqrt{\theta_{Mi}^2+\theta_{\min}^2}\tanh\left(k_g\theta_{Mi}\right) \tag{15}$$

where $\theta_{\min} > 0$ is a small dead-zone smoothing threshold and $k_g > 0$ governs the transition steepness. The mismatch between the nominal and smoothed gains, $\tilde{G}_{ti} \triangleq G_{ti} - \bar{G}_{ti}$, is strictly bounded over the compact flight envelope. Note that $\bar{G}_{ti}$ still vanishes at the isolated instant $\theta_{Mi} = 0$: the mapping preserves feedback polarity and continuity (avoiding the chattering of $\mathrm{sgn}(\theta_{Mi})$ switching), the gain loss at the crossing is transient, and the dissipation bound in Section 3.2 is therefore taken outside the dead-zone threshold.

Consequently, the linear continuous distributed temporal consensus protocol u_{ti} is formulated as:

$$u_{ti} = -\bar{k}_t K_T \bar{G}_{ti}(\mathbf{x}_i) e_{ti} \tag{16}$$

where $K_T > 0$ is the temporal consensus master gain parameter to be synthesized, and $\bar{k}_t > 0$ is a baseline temporal scaling factor.

2.4 Definition of Cooperative Guidability

Under the prescribed protocol structure (7), (13), and (16), the controller synthesis degrees of freedom are condensed into the two-dimensional master gain vector $\mathbf{K} \triangleq (K_S, K_T) \in \mathbb{R}_+^2$.

Missile salvo guidance is inherently a finite-horizon control problem. Let $T_f \geq \min_i(R_{i0}/V_{Mi})$ denote the available flight horizon of the salvo group, $v_0 = \|\mathbf{v}(0)\|_2$ the initial aggregate error energy envelope, and $\epsilon > 0$ the maximum permissible terminal error tolerance at interception ($t = T_f$). Requiring the error envelope to decay below ϵ prior to impact ($v(T_f) \leq v_0 e^{-\sigma_0 T_f} \leq \epsilon$) dictates a mandatory minimum finite-horizon exponential decay rate threshold σ_0:

$$\sigma_0 \triangleq \frac{1}{T_f}\ln\left(\frac{v_0}{\epsilon}\right) > 0 \tag{17}$$

We now state the formal mathematical definition of Cooperative Guidability:

Definition 1 (Cooperative Guidability)**.** *Consider the multi-missile kinematics (2) with initial state $\mathbf{X}(0)$, communication graph $\mathcal{G}$, maximum physical lateral overload $a_{\max}$, and the composite control protocol (13) and (16). Define two gain sets in the parameter space $\mathbb{R}_+^2$:*

1. ***Theoretical Convergence Gain Set*** $\mathcal{K}_{theory}(\sigma_0)$***:*** *The set of gain pairs (K_S, K_T) that guarantee asymptotic stability of the interconnected closed-loop system with an exponential envelope decay rate of at least σ_0 (or ultimate boundedness within tolerance ϵ under disturbances, where $\epsilon_{res} \geq 0$ denotes the residual bound and $\epsilon_{res} = 0$ in the ideal case):*

$$\mathcal{K}_{theory}(\sigma_0) \triangleq \Big\{(K_S,K_T)\in\mathbb{R}_+^2 \;\Big|\; \|\mathbf{v}(t)\|_2 \leq \|\mathbf{v}(0)\|_2 e^{-\sigma_0 t} + \epsilon_{res},\ \forall t\in[0,T_f]\Big\} \tag{18}$$

2. ***Physical Overload Admissible Gain Set*** $\mathcal{K}_{physical}(a_{\max})$***:*** *The set of gain pairs (K_S, K_T) under which the peak composite lateral acceleration command never violates the physical saturation limit over the entire engagement horizon:*

$$\mathcal{K}_{physical}(a_{\max}) \triangleq \Big\{(K_S,K_T)\in\mathbb{R}_+^2 \;\Big|\; \sup_{t\in[0,T_f]}\max_{i\in\mathcal{V}}|u_{qi}(K_S,t)+u_{ti}(K_T,t)| \leq a_{\max}\Big\} \tag{19}$$

The multi-missile system is defined as ***Cooperatively Guidable*** *under the given scenario and protocol structure if and only if the Parameter Feasibility Space is non-empty:*

$$\mathcal{K}_{feasible} \triangleq \mathcal{K}_{theory}(\sigma_0) \cap \mathcal{K}_{physical}(a_{\max}) \neq \emptyset \tag{20}$$

Conversely, if $\mathcal{K}_{feasible} = \emptyset$, the system is classified as ***Structurally Unguidable****.*

3 Vector Lyapunov Stability Analysis and Closed-Form Optimal Gain Synthesis

To analytically delineate the boundaries of $\mathcal{K}_{\text{theory}}(\sigma_0)$ and $\mathcal{K}_{\text{physical}}(a_{\max})$, we decompose the large-scale interconnected system into the spatial angle subsystem Σ_1 and the temporal consensus subsystem Σ_2, constructing a two-dimensional Vector Lyapunov Function $\mathbf{V} = [V_1, V_2]^T$.

3.1 Lyapunov Derivative and Interconnection Bounding for Spatial Subsystem Σ_1

Define the aggregate Lyapunov function for the spatial subsystem Σ_1 as the sum of individual logarithmic BLFs:

$$V_1(\mathbf{z}_1,\mathbf{z}_2) \triangleq \sum_{i=1}^{n} V_{1i} = \sum_{i=1}^{n}\left[\frac{1}{2}z_{1i}^2 + \frac{1}{2}\ln\left(\frac{k_b^2}{k_b^2 - z_{2i}^2}\right)\right] \tag{21}$$

Under ideal kinematics ($d_{qi} = 0$, with disturbances analyzed in Section 4), differentiating V_{1i} along (2)

and (10) step-by-step yields:

$$\begin{aligned}\dot{V}_{1i} &= z_{1i}\dot{z}_{1i} + \frac{z_{2i}}{k_b^2 - z_{2i}^2}\dot{z}_{2i} \\ &= z_{1i}\left[-\frac{V_{Mi}}{R_i}(\alpha_i + z_{2i})\right] \\ &\quad + \frac{z_{2i}}{k_b^2 - z_{2i}^2}\left[\cos\theta_{Mi}\left(\frac{u_{qi}+u_{ti}}{V_{Mi}} + \frac{V_{Mi}\sin\theta_{Mi}}{R_i}\right) - \dot{\alpha}_i\right] \\ &= -\frac{V_{Mi}}{R_i}z_{1i}\alpha_i - \frac{V_{Mi}}{R_i}z_{1i}z_{2i} \\ &\quad + \frac{z_{2i}}{k_b^2 - z_{2i}^2}\left[\frac{\cos\theta_{Mi}}{V_{Mi}}u_{qi} + \frac{V_{Mi}\sin\theta_{Mi}\cos\theta_{Mi}}{R_i}\right. \\ &\quad \left. - \dot{\alpha}_i + \frac{\cos\theta_{Mi}}{V_{Mi}}u_{ti}\right] \end{aligned} \tag{22}$$

Substituting the spatial control law u_{qi} from (13) into (22), we observe that the barrier-weighted term $+\left(k_b^2 - z_{2i}^2\right)\frac{V_{Mi}}{R_i}z_{1i}$ inside $\frac{\cos\theta_{Mi}}{V_{Mi}}u_{qi}$, when multiplied by the outer factor $\frac{z_{2i}}{k_b^2 - z_{2i}^2}$, simplifies to $+\frac{V_{Mi}}{R_i}z_{1i}z_{2i}$. This **algebraically cancels** the cross-coupling singular term $-\frac{V_{Mi}}{R_i}z_{1i}z_{2i}$! Consequently, (22) reduces cleanly to:

$$\begin{aligned}\dot{V}_{1i} = &-\frac{V_{Mi}}{R_i}z_{1i}\lambda_0\tanh\left(\bar{k}_1 K_S R_i z_{1i}\right) - \frac{\bar{k}_2 K_S}{k_b^2 - z_{2i}^2}z_{2i}^2 \\ &+ \frac{z_{2i}}{k_b^2 - z_{2i}^2}\frac{\cos\theta_{Mi}}{V_{Mi}}u_{ti}\end{aligned} \tag{23}$$

We now bound the three components on the right-hand side of (23):

1. *Outer-Loop Dissipation Bound:* Within any compact semi-global operating region Ω_0, the hyperbolic tangent function satisfies the sector lower bound $x\tanh(x) \geq c_0 x^2$ for some constant $c_0 \in (0,1)$. Thus:

$$-\frac{V_{Mi}}{R_i}z_{1i}\lambda_0\tanh\left(\bar{k}_1 K_S R_i z_{1i}\right) \leq -\left(c_0\lambda_0\bar{k}_1 V_{Mi}\right)K_S z_{1i}^2 \tag{24}$$

2. *Inner-Loop BLF Dissipation Bound:* By the fundamental logarithmic inequality $\ln\left(\frac{k_b^2}{k_b^2 - z_{2i}^2}\right) \leq \frac{z_{2i}^2}{k_b^2 - z_{2i}^2}$ for all $|z_{2i}| < k_b$ [22], we have:

$$-\frac{\bar{k}_2 K_S}{k_b^2 - z_{2i}^2}z_{2i}^2 \leq -\bar{k}_2 K_S \ln\left(\frac{k_b^2}{k_b^2 - z_{2i}^2}\right) \tag{25}$$

Combining (24) and (25) and defining the intrinsic spatial dissipation coefficient $\eta_1 \triangleq \min_i\left\{c_0\lambda_0\bar{k}_1 V_{Mi},\ \bar{k}_2\right\} > 0$, the sum of the first two terms across all n missiles satisfies:

$$\sum_{i=1}^{n}\left[-\frac{V_{Mi}}{R_i}z_{1i}\alpha_i - \frac{\bar{k}_2 K_S}{k_b^2 - z_{2i}^2}z_{2i}^2\right] \leq -2\eta_1 K_S V_1 \tag{26}$$

3. *Temporal-to-Spatial Interconnected Perturbation Bound:* Within the invariant interior $|z_{2i}| \leq \rho_z k_b$ ($\rho_z \in (0,1)$), we have $\frac{|z_{2i}|}{k_b^2 - z_{2i}^2} \leq \frac{\sqrt{2}}{k_b(1-\rho_z^2)}\sqrt{V_{1i}}$. Substituting $|u_{ti}| = \bar{k}_t K_T|\bar{G}_{ti}||e_{ti}|$ and applying the Cauchy-Schwarz inequality alongside Lemma 1 ($\|\mathbf{e}_T\|_2 \leq \sqrt{\frac{2}{\lambda_2(L)}}\sqrt{V_2}$), there exists a geometry-dependent cross-coupling coefficient $\gamma_{12} \triangleq \max_i \frac{\bar{k}_t \sup|\bar{G}_{ti}|}{V_{Mi}k_b(1-\rho_z^2)\sqrt{\lambda_2(L)}} > 0$ such that:

$$\sum_{i=1}^{n}\frac{z_{2i}}{k_b^2 - z_{2i}^2}\frac{\cos\theta_{Mi}}{V_{Mi}}u_{ti} \leq 2\gamma_{12}K_T\sqrt{V_1}\sqrt{V_2} \tag{27}$$

Combining (26) and (27) yields the differential inequality for the spatial subsystem Σ_1:

$$\dot{V}_1 \leq -2\eta_1 K_S V_1 + 2\gamma_{12}K_T\sqrt{V_1}\sqrt{V_2} \tag{28}$$

3.2 Lyapunov Derivative and Interconnection Bounding for Temporal Subsystem Σ_2

For the temporal consensus error vector $\mathbf{e}_T = L\mathbf{t}_{go}$, since $L = L^T \geq 0$ and $\mathbf{1}_n^T\mathbf{e}_T = \mathbf{1}_n^T L\mathbf{t}_{go} = 0$, we construct the temporal Lyapunov function as:

$$V_2(\mathbf{e}_T) \triangleq \frac{1}{2}\mathbf{e}_T^T L\mathbf{e}_T \tag{29}$$

By Lemma 1, since $\mathbf{e}_T \perp \mathbf{1}_n$, V_2 is strictly positive definite on the consensus manifold and satisfies:

$$\frac{1}{2}\lambda_2(L)\|\mathbf{e}_T\|_2^2 \leq V_2(\mathbf{e}_T) \leq \frac{1}{2}\lambda_n(L)\|\mathbf{e}_T\|_2^2 \tag{30}$$

Differentiating $\mathbf{e}_T$ along (6) (noting that $L\mathbf{1}_n = \mathbf{0}$ annihilates the constant -1 term) yields:

$$\begin{aligned}\dot{\mathbf{e}}_T &= L\dot{\mathbf{t}}_{go} = L\left[-\mathbf{1}_n + \mathbf{G}(\mathbf{u}_q + \mathbf{u}_t) + \boldsymbol{\Delta} + \mathbf{d}_t\right] \\ &= L\mathbf{G}\mathbf{u}_t + L\mathbf{G}\mathbf{u}_q + L(\boldsymbol{\Delta} + \mathbf{d}_t)\end{aligned} \tag{31}$$

where $\mathbf{G} = \mathrm{diag}\{G_{t1}, \ldots, G_{tn}\}$ and $\bar{\mathbf{G}} = \mathrm{diag}\{\bar{G}_{t1}, \ldots, \bar{G}_{tn}\}$. Substituting $\mathbf{u}_t = -\bar{k}_t K_T\bar{\mathbf{G}}\mathbf{e}_T$ into $\dot{V}_2 = \mathbf{e}_T^T L\dot{\mathbf{e}}_T$ under ideal conditions ($\boldsymbol{\Delta} = \mathbf{0}, \mathbf{d}_t = \mathbf{0}, \tilde{\mathbf{G}} = \mathbf{0}$) gives:

$$\dot{V}_2 = -\bar{k}_t K_T\mathbf{e}_T^T L^2\bar{\mathbf{G}}^2\mathbf{e}_T + \mathbf{e}_T^T L^2\mathbf{G}\mathbf{u}_q \tag{32}$$

We bound the two terms on the right-hand side of (32) as follows:

1. *Intrinsic Temporal Dissipation Term:* Outside the smoothed dead-zone threshold, $|\bar{G}_{ti}| \geq g_{\min} > 0$. Utilizing (1) and (30) where $\mathbf{e}_T^T L^2 \mathbf{e}_T \geq \lambda_2(L)\mathbf{e}_T^T L \mathbf{e}_T = 2\lambda_2(L)V_2$, and defining the intrinsic temporal dissipation coefficient $\eta_2 \triangleq \bar{k}_t g_{\min}^2 > 0$, we obtain:

$$-\bar{k}_t K_T \mathbf{e}_T^T L^2 \bar{\mathbf{G}}^2 \mathbf{e}_T \leq -2\eta_2 \lambda_2(L) K_T V_2 \tag{33}$$

2. *Spatial-to-Temporal Interconnected Perturbation Term:* From (13) and (11), the dominant feedback terms in u_{qi} scale linearly with the spatial master gain K_S and the spatial error norm, satisfying $\|\mathbf{u}_q\|_2 \leq \bar{\phi}_q K_S \sqrt{V_1}$. Consequently, there exists a coupling constant $\gamma_{21} \triangleq \frac{\lambda_n^{3/2}(L)\sup|G_{ti}|\bar{\phi}_q}{\sqrt{2}} > 0$ such that:

$$\mathbf{e}_T^T L^2 \mathbf{G} \mathbf{u}_q \leq 2\gamma_{21} K_S \sqrt{V_2}\sqrt{V_1} \tag{34}$$

Combining (33) and (34) yields the differential inequality for the temporal subsystem Σ_2:

$$\dot{V}_2 \leq -2\eta_2 \lambda_2(L) K_T V_2 + 2\gamma_{21} K_S \sqrt{V_2}\sqrt{V_1} \tag{35}$$

3.3 Large-Scale Comparison Principle and Shifted M-Matrix Transformation

Applying the square-root state transformation $\mathbf{v}(t) = [v_1(t), v_2(t)]^T \triangleq [\sqrt{V_1(t)}, \sqrt{V_2(t)}]^T$ and noting that $\dot{v}_k = \frac{\dot{V}_k}{2\sqrt{V_k}}$ $(k = 1, 2)$, dividing (28) and (35) by $2\sqrt{V_1}$ and $2\sqrt{V_2}$ respectively yields the **interconnected linear comparison differential inequality system**:

$$\begin{bmatrix} \dot{v}_1(t) \\ \dot{v}_2(t) \end{bmatrix} \leq -\underbrace{\begin{bmatrix} \eta_1 K_S & -\gamma_{12} K_T \\ -\gamma_{21} K_S & \eta_2 \lambda_2(L) K_T \end{bmatrix}}_{M(K_S, K_T)} \begin{bmatrix} v_1(t) \\ v_2(t) \end{bmatrix} \tag{36}$$

where $M(K_S, K_T)$ is a Z-matrix (off-diagonal elements are non-positive).

To enforce the finite-horizon decay rate threshold σ_0 required by Definition 1 ($\|\mathbf{v}(t)\|_2 \leq \|\mathbf{v}(0)\|_2 e^{-\sigma_0 t}$), we introduce the exponential time-shifted state $\mathbf{w}(t) \triangleq e^{\sigma_0 t}\mathbf{v}(t)$. Differentiating $\mathbf{w}(t)$ and substituting (36) yields:

$$\begin{aligned} \dot{\mathbf{w}}(t) &= \sigma_0 e^{\sigma_0 t}\mathbf{v}(t) + e^{\sigma_0 t}\dot{\mathbf{v}}(t) \\ &\leq -\left[M(K_S, K_T) - \sigma_0 I_2\right]\mathbf{w}(t) \triangleq -M_{\sigma_0}(K_S, K_T)\mathbf{w}(t) \end{aligned} \tag{37}$$

where the **shifted comparison matrix** $M_{\sigma_0}(K_S, K_T)$ is given explicitly by:

$$M_{\sigma_0}(K_S, K_T) = \begin{bmatrix} \eta_1 K_S - \sigma_0 & -\gamma_{12} K_T \\ -\gamma_{21} K_S & \eta_2 \lambda_2(L) K_T - \sigma_0 \end{bmatrix} \tag{38}$$

By the Vector Lyapunov Comparison Principle [25, 26] and the leading principal minor criterion for non-singular M-matrices, $\mathbf{w}(t)$ is asymptotically bounded (meaning $\mathbf{v}(t)$ decays exponentially at a rate no less than σ_0) **if and only if** $M_{\sigma_0}(K_S, K_T)$ is a non-singular M-matrix:

$$\begin{aligned} \mathcal{K}_{\text{theory}}(\sigma_0) = \Big\{ (K_S, K_T) \in \mathbb{R}_+^2 \;\Big|\; & \eta_1 K_S - \sigma_0 > 0, \\ & \eta_2 \lambda_2(L) K_T - \sigma_0 > 0, \text{ and } \det\left(M_{\sigma_0}(K_S, K_T)\right) \\ & = (\eta_1 K_S - \sigma_0)(\eta_2 \lambda_2(L) K_T - \sigma_0) \\ & - \gamma_{12}\gamma_{21} K_S K_T \geq 0 \Big\} \end{aligned} \tag{39}$$

3.4 Closed-Form Optimal Gain Synthesis via AM-GM Extremum Optimization

Simultaneously, physical actuator saturation (19) requires the peak composite command to remain within $a_{\max}$. Let $\Phi_S(z_0)$ and $\Phi_T(e_{t0})$ denote the command sensitivity envelopes determined by the initial spatial and temporal errors such that $\sup|u_{qi}| = \Phi_S(z_0)K_S$ and $\sup|u_{ti}| = \Phi_T(e_{t0})K_T$. The physical overload admissible set is then expressed as:

$$\begin{aligned} \mathcal{K}_{\text{physical}}(a_{\max}) = \big\{ (K_S, K_T) \in \mathbb{R}_+^2 \;\big|\; & \Phi_S(z_0)K_S \\ & + \Phi_T(e_{t0})K_T \leq a_{\max} \big\} \end{aligned} \tag{40}$$

To determine whether $\mathcal{K}_{\text{theory}}(\sigma_0) \cap \mathcal{K}_{\text{physical}}(a_{\max}) \neq \emptyset$ and solve for the optimal gains, we execute a four-step dimensionless extremum optimization procedure:

Step 1 (*Extraction of Characteristic Physical Parameters*)
Define the **dimensionless spatiotemporal coupling intensity** ρ, the **baseline spatial overload demand** A_S, and the **baseline temporal overload demand** A_T:

$$\rho \triangleq \frac{\gamma_{12}\gamma_{21}}{\eta_1 \eta_2 \lambda_2(L)}, \quad A_S \triangleq \frac{\sigma_0 \Phi_S(z_0)}{\eta_1}, \quad A_T \triangleq \frac{\sigma_0 \Phi_T(e_{t0})}{\eta_2 \lambda_2(L)} \tag{41}$$

Step 2 (*Dimensionless Coordinate Transformation and Hyperbolic Completion of Squares*)
Introduce the dimensionless normalized gain coordinates:

$$x \triangleq \frac{\eta_1 K_S}{\sigma_0} > 1, \quad y \triangleq \frac{\eta_2 \lambda_2(L) K_T}{\sigma_0} > 1 \tag{42}$$

Substituting (42) into the determinant condition $\det(M_{\sigma_0}) \geq 0$ in (39) and dividing both sides by $\sigma_0^2 > 0$ yields:

$$\begin{aligned} (x-1)(y-1) &\geq \frac{\gamma_{12}\gamma_{21}}{\eta_1 \eta_2 \lambda_2(L)} xy = \rho xy \\ \iff (1-\rho)xy - x - y + 1 &\geq 0 \end{aligned} \tag{43}$$

When $0 \leq \rho < 1$, dividing both sides of (43) by $(1-\rho) > 0$ and completing the rectangle for x and y step-by-step gives:

$$\begin{aligned} & xy - \frac{x}{1-\rho} - \frac{y}{1-\rho} + \frac{1}{(1-\rho)^2} \geq \frac{1}{(1-\rho)^2} - \frac{1}{1-\rho} \\ \iff & \left(x - \frac{1}{1-\rho}\right)\left(y - \frac{1}{1-\rho}\right) \geq \frac{\rho}{(1-\rho)^2} \end{aligned} \tag{44}$$

Defining the shifted excess variables $\Delta x \triangleq x - \frac{1}{1-\rho} > 0$ and $\Delta y \triangleq y - \frac{1}{1-\rho} > 0$, the stability boundary is rigorously transformed into a **rectangular hyperbola**: $\Delta x \cdot \Delta y \geq \frac{\rho}{(1-\rho)^2}$.

Step 3 (*Minimum Peak Overload Extremum Optimization*) In the (x, y) plane, the composite peak overload cost function is $J(x,y) \triangleq \Phi_S K_S + \Phi_T K_T = A_S x + A_T y$. Substituting $x = \frac{1}{1-\rho} + \Delta x$ and $y = \frac{1}{1-\rho} + \Delta y$ into $J(x,y)$ and applying the Arithmetic-Geometric Mean (AM-GM) inequality subject to the hyperbolic constraint $\Delta x \cdot \Delta y \geq \frac{\rho}{(1-\rho)^2}$ yields the global minimum required overload:

$$\begin{aligned} J(x,y) &= \frac{A_S + A_T}{1-\rho} + (A_S \Delta x + A_T \Delta y) \\ &\geq \frac{A_S + A_T}{1-\rho} + 2\sqrt{A_S A_T (\Delta x \cdot \Delta y)} \\ &\geq \frac{A_S + A_T + 2\sqrt{\rho A_S A_T}}{1-\rho} \triangleq a_{\text{req, min}} \end{aligned} \tag{45}$$

Step 4 (*Closed-Form Inversion for Optimal Gains*) Equality in the AM-GM inequality (45) holds if and only if $A_S \Delta x^* = A_T \Delta y^*$ and $\Delta x^* \Delta y^* = \frac{\rho}{(1-\rho)^2}$. Solving these two equations simultaneously yields the unique optimal dimensionless increments:

$$\Delta x^* = \frac{\sqrt{\rho}}{1-\rho}\sqrt{\frac{A_T}{A_S}}, \quad \Delta y^* = \frac{\sqrt{\rho}}{1-\rho}\sqrt{\frac{A_S}{A_T}} \tag{46}$$

Mapping (46) back to the physical gain space via (42) produces the closed-form analytical solution for the **globally unique optimal control gain saddle point** (K_S^*, K_T^*):

$$\begin{aligned} K_S^* &= \frac{\sigma_0}{\eta_1(1-\rho)}\left(1 + \sqrt{\frac{\rho A_T}{A_S}}\right) \\ K_T^* &= \frac{\sigma_0}{\eta_2 \lambda_2(L)(1-\rho)}\left(1 + \sqrt{\frac{\rho A_S}{A_T}}\right) \end{aligned} \tag{47}$$

4 Necessary and Sufficient Conditions for Cooperative Guidability Across Three Scenarios

Building upon the mathematical machinery of Section 3, we establish the necessary and sufficient Cooperative Guidability theorems for the ideal, uncertain, and disturbed scenarios.

4.1 Scenario 1: Ideal Kinematics (Two-Sided Hyperbolic-Linear Squeeze Criterion)

Theorem 1 (Necessary and Sufficient Condition for Ideal Cooperative Guidability)**.** *Consider the multi-missile system (2) under ideal kinematics ($\Delta_i = 0, d_{qi} = d_{ti} = 0$). Under the composite protocol (13) and (16), the system is Cooperatively Guidable in the VLF envelope sense ($\mathcal{K}_{feasible} \neq \emptyset$) and achieves finite-horizon temporal consensus ($\max_{i,j\in\mathcal{V}} |t_{go,i}(T_f) - t_{go,j}(T_f)| \leq \epsilon_{sync}$) **if and only if** the following three algebraic conditions hold simultaneously:*

1. ***Topological Connectivity and Structural Decoupling Condition:*** *The communication graph $\mathcal{G}$ is connected ($\lambda_2(L) > 0$), and the dimensionless spatiotemporal coupling intensity is strictly less than unity:*

$$\rho = \frac{\gamma_{12}\gamma_{21}}{\eta_1 \eta_2 \lambda_2(L)} < 1 \tag{48}$$

2. ***Overload Margin Necessary and Sufficient Condition:*** *The dimensionless **Ideal Cooperative Guidability Index** Ξ_{CG}^{ideal} does not exceed unity:*

$$\Xi_{CG}^{ideal} \triangleq \frac{A_S + A_T + 2\sqrt{\rho A_S A_T}}{(1-\rho) a_{\max}} \leq 1 \tag{49}$$

3. ***Finite-Horizon Temporal Consensus Synchronization and Connectivity Condition:*** *Given a prescribed terminal impact-time synchronization tolerance $\epsilon_{sync} > 0$ (with consensus error tolerance $\epsilon_t = \lambda_2(L)\epsilon_{sync}/\sqrt{2}$), the spatial overload demand satisfies $A_S < a_{\max}$, the decay rate threshold satisfies $\sigma_0 \geq \sigma_{T,sync} \triangleq \frac{1}{T_f} \ln\left(\frac{2v_0}{\lambda_2^{3/2}(L)\epsilon_{sync}}\right)$, the effective coupled temporal consensus dissipation rate satisfies:*

$$\begin{aligned} & \sigma_{T,eff}(K_S, K_T) \triangleq \eta_2 \lambda_2(L) K_T - \frac{\gamma_{12}\gamma_{21} K_S K_T}{\eta_1 K_S - \sigma_0} \\ & \geq \sigma_0 \geq \sigma_{T,sync} \end{aligned} \tag{50}$$

and the network algebraic connectivity $\lambda_2(L)$ exceeds

the critical temporal consensus threshold:

$$\lambda_2(L) \geq \lambda_{2,\min}^{ideal} \triangleq \frac{\bar{\rho} a_{\max} + \bar{A}_T + 2\sqrt{\bar{\rho} A_S \bar{A}_T}}{a_{\max} - A_S} \tag{51}$$

where $\bar{\rho} \triangleq \frac{\gamma_{12}\gamma_{21}}{\eta_1\eta_2}$ *and* $\bar{A}_T \triangleq \frac{\sigma_0 \Phi_T(e_{t0})}{\eta_2}$. *Furthermore, when Conditions 1-3 hold, the inter-missile time-to-go disagreement* $\tilde{\mathbf{t}}_{go}(t) \triangleq \left(I_n - \frac{1}{n}\mathbf{1}_n\mathbf{1}_n^T\right)\mathbf{t}_{go}(t)$ *and pairwise impact-time synchronization error converge exponentially according to:*

$$\max_{i,j\in\mathcal{V}} |t_{go,i}(t) - t_{go,j}(t)| \leq \sqrt{2}\|\tilde{\mathbf{t}}_{go}(t)\|_2 \leq \frac{2v_0}{\lambda_2^{3/2}(L)} e^{-\sigma_0 t} \leq \epsilon_{sync}, \quad \forall t \geq T_f \tag{52}$$

Proof. Necessity ($\Longrightarrow$)*:* Suppose $\mathcal{K}_{\text{feasible}} \neq \emptyset$, so there exists $(K_S, K_T) \in \mathcal{K}_{\text{theory}}(\sigma_0) \cap \mathcal{K}_{\text{physical}}(a_{\max})$. First, if $\mathcal{G}$ is disconnected ($\lambda_2(L) = 0$), the $(2,2)$ entry of M_{σ_0} is $-\sigma_0 < 0$, violating the M-matrix condition. If $\rho \geq 1$, then for any $x > 1, y > 1$, $(1-\rho)xy - x - y + 1 \leq -(x + y - 1) < -1 < 0$, contradicting (43); hence $\rho < 1$ is strictly necessary. Second, since $(x, y) \in \mathcal{K}_{\text{theory}}(\sigma_0)$ and satisfies $J(x, y) \leq a_{\max}$, the global minimum property (45) implies $a_{\text{req, min}} \leq J(x, y) \leq a_{\max}$. Dividing by $a_{\max}$ yields $\Xi_{\text{CG}}^{\text{ideal}} \leq 1$. Third, regarding the temporal consensus condition, since $\eta_1 K_S - \sigma_0 > 0$, taking the Schur complement of the $(1,1)$ entry in $\det(M_{\sigma_0}(K_S, K_T)) \geq 0$ in (39) directly yields the effective coupled temporal dissipation rate condition $\sigma_{T,\text{eff}}(K_S, K_T) = \eta_2\lambda_2(L)K_T - \frac{\gamma_{12}\gamma_{21}K_S K_T}{\eta_1 K_S - \sigma_0} \geq \sigma_0$. Moreover, substituting $\rho = \bar{\rho}/\lambda_2(L)$ and $\bar{A}_T = \bar{A}_T/\lambda_2(L)$ into $\Xi_{\text{CG}}^{\text{ideal}} \leq 1$ yields $A_S + \frac{\bar{A}_T}{\lambda_2(L)} + \frac{2\sqrt{\bar{\rho} A_S \bar{A}_T}}{\lambda_2(L)} \leq \left(1 - \frac{\bar{\rho}}{\lambda_2(L)}\right) a_{\max}$, which necessitates $A_S < a_{\max}$ and rearranges directly into the minimum connectivity condition $\lambda_2(L) \geq \lambda_{2,\min}^{\text{ideal}}$ in (51).

Sufficiency ($\Longleftarrow$)*:* Suppose (48), (49), and (50)-(51) hold. Select the optimal gain pair (K_S^*, K_T^*) given by (47). By construction, its normalized coordinates (x^*, y^*) lie on the hyperbolic boundary $(x^* - 1)(y^* - 1) = \rho x^* y^*$ with $x^* > \frac{1}{1-\rho} > 1$ and $y^* > \frac{1}{1-\rho} > 1$, confirming $\sigma_{T,\text{eff}}(K_S^*, K_T^*) = \sigma_0 \geq \sigma_{T,\text{sync}}$ and $(K_S^*, K_T^*) \in \mathcal{K}_{\text{theory}}(\sigma_0)$. Furthermore, its peak composite overload satisfies $\Phi_S K_S^* + \Phi_T K_T^* = a_{\text{req, min}} = \Xi_{\text{CG}}^{\text{ideal}} a_{\max} \leq a_{\max}$, confirming $(K_S^*, K_T^*) \in \mathcal{K}_{\text{physical}}(a_{\max})$. Thus, $\mathcal{K}_{\text{feasible}} \neq \emptyset$. Finally, since the time-to-go disagreement vector $\tilde{\mathbf{t}}_{go} = \left(I_n - \frac{1}{n}\mathbf{1}_n\mathbf{1}_n^T\right)\mathbf{t}_{go}$ satisfies $\mathbf{1}_n^T\tilde{\mathbf{t}}_{go} = 0$ and $\mathbf{e}_T = L\tilde{\mathbf{t}}_{go}$, Lemma 1 and (30) imply $V_2(\mathbf{e}_T) = \frac{1}{2}\tilde{\mathbf{t}}_{go}^T L^3 \tilde{\mathbf{t}}_{go} \geq \frac{1}{2}\lambda_2^3(L)\|\tilde{\mathbf{t}}_{go}\|_2^2$. Consequently, $\max_{i,j} |t_{go,i}(t) - t_{go,j}(t)| \leq \sqrt{2}\|\tilde{\mathbf{t}}_{go}(t)\|_2 \leq \frac{2}{\lambda_2^{3/2}(L)} v_2(t) \leq \frac{2v_0}{\lambda_2^{3/2}(L)} e^{-\sigma_0 t}$. Evaluating at $t = T_f$ with $\sigma_0 \geq \sigma_{T,\text{sync}}$ confirms (52). □

4.2 Scenario 2: Internal Parametric Uncertainties and Dead-Zone Mismatch

In practical engagements, aerodynamic parameter variations and the dead-zone smoothing mismatch $\tilde{G}_{ti} = G_{ti} - \bar{G}_{ti}$ manifest as two types of internal uncertainties:

1. *Multiplicative Control Gain Uncertainty:* The actual temporal gain satisfies $G_{ti}\bar{G}_{ti} \geq (1-\delta_G)\bar{G}_{ti}^2$, where $\delta_G \in [0, 1)$ denotes the maximum multiplicative relative deviation;
2. *Additive Unmodeled Dynamics:* The high-order Taylor truncation residual and aerodynamic damping perturbations in (6) are bounded by $|\Delta_i(t)| \leq \delta_{\text{unc}}$, implying $\|\boldsymbol{\Delta}(t)\|_2 \leq \sqrt{n}\delta_{\text{unc}}$.

Substituting these uncertainties into the temporal Lyapunov derivative (32) and bounding the additive perturbation via $\mathbf{e}_T^T L\boldsymbol{\Delta} \leq \frac{\sqrt{2n}\lambda_n(L)\delta_{\text{unc}}}{\sqrt{\lambda_2(L)}} v_2$, the comparison system (36) becomes:

$$\begin{bmatrix}\dot{v}_1 \\ \dot{v}_2\end{bmatrix} \leq -\underbrace{\begin{bmatrix}\eta_1 K_S & -\gamma_{12}K_T \\ -\gamma_{21}K_S & \eta_2(1-\delta_G)\lambda_2(L)K_T\end{bmatrix}}_{M_{\text{unc}}(K_S,K_T)} \begin{bmatrix}v_1 \\ v_2\end{bmatrix} + \begin{bmatrix}0 \\ \bar{d}_{\text{unc}}\end{bmatrix} \tag{53}$$

where $\bar{d}_{\text{unc}} \triangleq \frac{\lambda_n(L)\sqrt{n}\delta_{\text{unc}}}{\sqrt{2\lambda_2(L)}}$ is the effective uncertainty excitation amplitude.

Theorem 2 (Necessary and Sufficient Condition for Uncertain Cooperative Guidability)**.** *Under multiplicative gain uncertainty* δ_G *and additive unmodeled dynamics* δ_{unc}*, define the* ***inflated coupling intensity*** ρ_{unc} *and the* ***inflated baseline overload demands*** (A_S^{unc}, A_T^{unc})*:*

$$\rho_{unc} \triangleq \frac{\rho}{1-\delta_G} = \frac{\gamma_{12}\gamma_{21}}{\eta_1\eta_2(1-\delta_G)\lambda_2(L)}$$
$$A_T^{unc} \triangleq \frac{\sigma_{unc}}{\sigma_0(1-\delta_G)} A_T, \quad A_S^{unc} \triangleq \frac{\sigma_{unc}}{\sigma_0} A_S \tag{54}$$

where $\sigma_{unc} \triangleq \max\left\{\frac{1}{T_f}\ln\left(\frac{2v_0}{\epsilon}\right), \frac{2\bar{d}_{unc}}{\epsilon\sqrt{\lambda_2(L)/2}}\right\}$ *is the enhanced decay rate threshold required to simultaneously suppress transient initial errors and steady-state residuals. The system is Robustly Cooperatively Guidable and achieves practical temporal consensus within tolerance* $\epsilon_{sync}^{unc} = \frac{\sqrt{2}\epsilon_t}{\lambda_2(L)}$ ***if and only if****:*

$$\rho_{unc} < 1 \quad \textit{and} \quad \Xi_{CG}^{unc} \triangleq \frac{A_S^{unc} + A_T^{unc} + 2\sqrt{\rho_{unc} A_S^{unc} A_T^{unc}}}{(1-\rho_{unc})a_{\max}} \leq 1 \tag{55}$$

and the temporal consensus gain K_T and algebraic connectivity $\lambda_2(L)$ satisfy the uncertain temporal consensus conditions:

$$K_T \geq K_{T,\min}^{unc} \tag{56}$$

$$\triangleq \frac{\eta_1 \bar{d}_{unc}}{\left(\eta_1\eta_2(1-\delta_G)\lambda_2(L) - \gamma_{12}\gamma_{21}\right)\sqrt{\frac{\lambda_2(L)}{2}}\left(\epsilon_t - \frac{\epsilon}{2}\right)} \tag{57}$$

$$\lambda_2(L) \geq \lambda_{2,\min}^{unc} \triangleq \frac{\bar{\rho}a_{\max} + \frac{\sigma_{unc}}{\sigma_0}\bar{A}_T + 2\sqrt{\bar{\rho}A_S^{unc}\frac{\sigma_{unc}}{\sigma_0}\bar{A}_T}}{(1-\delta_G)\left(a_{\max} - A_S^{unc}\right)} \tag{58}$$

Furthermore, when (55)-(58) hold, the ultimate steady-state residual of the temporal consensus error vector and the pairwise impact-time synchronization discrepancy are bounded by:

$$\begin{aligned}
&\lim_{t\to T_f} \|\mathbf{e}_T(t)\|_2 \\
&\leq \sqrt{\frac{2}{\lambda_2(L)}}\left[\frac{\eta_1\bar{d}_{unc}}{\left(\eta_1\eta_2(1-\delta_G)\lambda_2(L) - \gamma_{12}\gamma_{21}\right)K_T}\right] + \frac{\epsilon}{2} \\
&\leq \epsilon_t
\end{aligned} \tag{59}$$

$$\begin{aligned}
&\lim_{t\to T_f}\max_{i,j\in\mathcal{V}}|t_{go,i}(t) - t_{go,j}(t)| \\
&\leq \frac{2}{\lambda_2^{3/2}(L)}\left[\frac{\eta_1\bar{d}_{unc}}{\left(\eta_1\eta_2(1-\delta_G)\lambda_2(L) - \gamma_{12}\gamma_{21}\right)K_T}\right] \\
&\quad + \frac{\epsilon}{\sqrt{2}\lambda_2(L)} \\
&\leq \epsilon_{sync}^{unc}
\end{aligned} \tag{60}$$

Proof. Setting the right-hand side of (53) to zero to solve for the equilibrium envelope $(v_{1,\infty}, v_{2,\infty})$ yields $v_{1,\infty} \leq \frac{\gamma_{12}K_T}{\eta_1 K_S} v_{2,\infty}$ from the first row. Substituting this into the second row gives:

$$\left[\eta_2(1-\delta_G)\lambda_2(L)K_T - \frac{\gamma_{12}\gamma_{21}K_SK_T}{\eta_1K_S}\right] v_{2,\infty} \leq \bar{d}_{\text{unc}} \tag{61}$$

which directly yields (59) via (30). Replacing η_2 with $\eta_2(1-\delta_G)$ and σ_0 with σ_{unc} in Steps 1-4 of Section 3.4 immediately establishes (55). Furthermore, solving (59) for K_T so that the steady-state plus transient temporal consensus error does not exceed ϵ_t yields (57), while substituting $\rho_{\text{unc}} = \frac{\bar{\rho}}{(1-\delta_G)\lambda_2(L)}$ and $A_T^{\text{unc}} = \frac{\sigma_{\text{unc}}\bar{A}_T}{\sigma_0(1-\delta_G)\lambda_2(L)}$ into $\Xi_{\text{CG}}^{\text{unc}} \leq 1$ isolates the minimum connectivity condition (58). Finally, utilizing the Rayleigh quotient relation $\max_{i,j}|t_{go,i} - t_{go,j}| \leq \sqrt{2}\|\tilde{\mathbf{t}}_{go}\|_2 \leq \frac{\sqrt{2}}{\lambda_2(L)}\|\mathbf{e}_T\|_2$ in (59) directly proves the pairwise impact-time synchronization bound (60). □

4.3 Scenario 3: External Target Maneuver Disturbances

When the target executes evasive maneuvers ($|a_T(t)| \leq a_{T\max}$ with maximum normal evasive speed $\sup|v_{Ti\perp}(t)| = v_{T\perp\max}$), a non-vanishing disturbance $d_{qi}(t) = \frac{v_{Ti\perp}(t)}{R_i}$ is injected into the outer-loop LOS rate channel (2). Substituting $\dot{z}_{1i} = -\frac{V_{Mi}}{R_i}(\alpha_i + z_{2i}) + \frac{v_{Ti\perp}(t)}{R_i}$ into (22), the outer-loop dissipation term becomes:

$$\dot{V}_{1i,\text{outer}} = -\frac{z_{1i}}{R_i}\left[V_{Mi}\lambda_0\tanh\left(\bar{k}_1K_SR_iz_{1i}\right) - v_{Ti\perp}(t)\right] \tag{62}$$

Theorem 3 (Necessary and Sufficient Condition for Cooperative Guidability Under Target Maneuvers)**.** *Against an evasive target with maximum acceleration $a_{T\max}$ and maximum normal speed $v_{T\perp\max}$, the multi-missile system is Cooperatively Guidable and achieves disturbed temporal consensus **if and only if** the following four structural and algebraic criteria hold simultaneously:*

1. ***Kinematic Velocity Capture Necessary Condition:*** *The missile's virtual control velocity authority must strictly dominate the target's maximum normal evasive speed:*

$$V_{Mi}\lambda_0 > v_{T\perp\max}, \quad \forall i \in \mathcal{V} \tag{63}$$

2. ***Physical Overload Margin Necessary Condition:*** *The missile's maximum overload must strictly exceed the baseline navigation overload required to track the maneuvering target ($N_e \geq 3$ denoting the effective navigation ratio):*

$$a_{avail} \triangleq a_{\max} - N_e a_{T\max} > 0 \tag{64}$$

3. ***Disturbed Overload Margin Algebraic Necessary and Sufficient Condition:*** *The dimensionless **Disturbed Cooperative Guidability Index** Ξ_{CG}^{dist} does not exceed unity:*

$$\Xi_{CG}^{dist} \triangleq \frac{A_S^{dist} + A_T^{dist} + 2\sqrt{\rho_{unc}A_S^{dist}A_T^{dist}}}{(1-\rho_{unc})\left(a_{\max} - N_e a_{T\max}\right)} \leq 1 \tag{65}$$

4. ***Disturbed Temporal Consensus Disturbance Rejection and Connectivity Condition:*** *Let $\bar{d}_{t,man} \triangleq \frac{\lambda_n(L)\sqrt{n}\sup_{t,i}|d_{ti}(t)|}{\sqrt{2\lambda_2(L)}}$ denote the temporal consensus perturbation amplitude induced by the target maneuver $d_{ti}(t)$ in (6). To guarantee that the inter-missile impact-time disagreement converges within $\epsilon_{sync}^{dist} > 0$ despite asymmetric target-to-missile*

LOS maneuver projections ($L\mathbf{d}_t \neq \mathbf{0}$), the algebraic connectivity $\lambda_2(L)$ and effective disturbed temporal consensus rate $\sigma^{dist}_{T,eff}(K_S, K_T)$ must satisfy:

$$\lambda_2(L) \geq \lambda^{dist}_{2,\min} \tag{66}$$

$$\sigma^{dist}_{T,eff}(K_S,K_T) \triangleq \eta_2(1-\delta_G)\lambda_2(L)K_T - \frac{\gamma_{12}\gamma_{21}K_SK_T}{\eta_1 K_S - \sigma_{dist}} \geq \max\left\{\sigma_{dist}, \frac{4(\bar{d}_{unc}+\bar{d}_{t,man})}{\lambda_2^{3/2}(L)\epsilon^{dist}_{sync}}\right\} \tag{67}$$

where $A^{dist}_S \triangleq \frac{\sigma_{dist}}{\sigma_0}A_S$, $A^{dist}_T \triangleq \frac{\sigma_{dist}}{\sigma_0(1-\delta_G)}A_T$, $\bar{A}^{dist}_T \triangleq \lambda_2(L)(1-\delta_G)A^{dist}_T$, $\lambda^{dist}_{2,\min}$ is given by (58) with $a_{\max}$ replaced by a_{avail} and σ_{unc} replaced by σ_{dist}, and $\sigma_{dist} \geq \frac{1}{T_f}\ln\left(\frac{4v_0}{\lambda_2^{3/2}(L)\epsilon^{dist}_{sync}}\right)$, guaranteeing the terminal impact-time synchronization bound:

$$\lim_{t\to T_f}\max_{i,j\in\mathcal{V}}|t_{go,i}(t)-t_{go,j}(t)| \leq \frac{2(\bar{d}_{unc}+\bar{d}_{t,man})}{\lambda_2^{3/2}(L)\sigma^{dist}_{T,eff}(K_S,K_T)} + \frac{2v_0}{\lambda_2^{3/2}(L)}e^{-\sigma_{dist}T_f} \leq \epsilon^{dist}_{sync} \tag{68}$$

Proof. 1) If (63) is violated ($V_{Mi}\lambda_0 \leq v_{T\perp\max}$), a target executing orthogonal evasion with $\operatorname{sgn}(v_{Ti\perp}) = \operatorname{sgn}(z_{1i})$ and $|v_{Ti\perp}| = v_{T\perp\max}$ forces $V_{Mi}\lambda_0|\tanh(\cdot)| - |v_{Ti\perp}| < 0$ in (62) since $|\tanh(\cdot)| < 1$. This renders $\dot{V}_{1i,\text{outer}} > 0$ regardless of how large K_S is chosen, causing z_{1i} to diverge. Thus (63) is strictly necessary. 2) When (63) holds, the net outer-loop velocity authority is reduced to $V_{Mi}\lambda_0 - v_{T\perp\max} > 0$, while classical pursuit-evasion kinematics dictate that an overload margin of $N_e a_{T\max}$ must be reserved to null the target-induced LOS rate, reducing the available overload budget for spatiotemporal error correction to $a_{\text{avail}} = a_{\max} - N_e a_{T\max}$. Replacing $a_{\max}$ with a_{avail} in (45) directly establishes (65). 3) In the temporal subsystem (31), the target maneuver injects the differential temporal disturbance $L\mathbf{d}_t$, which satisfies $\mathbf{e}_T^T L\mathbf{d}_t \leq \sqrt{2}\bar{d}_{t,\text{man}}v_2(t)$ in $\dot{V}_2$. Augmenting $\bar{d}_{\text{unc}}$ to $\bar{d}_{\text{unc}} + \bar{d}_{t,\text{man}}$ in (53) and applying the Schur complement to $M_{\text{unc}}(K_S,K_T)$ yields the disturbed temporal dissipation rate $\sigma^{\text{dist}}_{T,\text{eff}}(K_S,K_T)$ in (67) and the ultimate bound $v_2(T_f) \leq \frac{\bar{d}_{\text{unc}}+\bar{d}_{t,\text{man}}}{\sigma^{\text{dist}}_{T,\text{eff}}(K_S,K_T)} + v_0 e^{-\sigma_{\text{dist}}T_f}$. Mapping $v_2(T_f)$ to the pairwise time-to-go disagreement via $\max_{i,j}|t_{go,i}-t_{go,j}| \leq \frac{2}{\lambda_2^{3/2}(L)}v_2$ and isolating $\lambda_2(L)$ from (65) establishes (68). □

4.4 Dual Graphical Rapid-Verification Criteria and Conservatism Discussion

Theorems 1-3 directly translate into two intuitive graphical verification tools for fire-control engineers:

1. **"Hyperbola-Line Guidability Lens" in the Gain Plane** (K_S, K_T)**:** Plotting the stability boundary hyperbola $\det(M_{\sigma_0}(K_S,K_T)) = 0$ and the overload saturation line $\Phi_S K_S + \Phi_T K_T = a_{\text{avail}}$ in the (K_S,K_T) plane reveals three distinct regimes: when $\Xi_{\text{CG}} < 1$, the line intersects the upper-right branch of the hyperbola, enclosing a convex **"Feasible Gain Lens ($\mathcal{K}_{\text{feasible}}$)"** containing the optimal saddle point (K_S^*, K_T^*); when $\Xi_{\text{CG}} = 1$, the line is tangent to the hyperbola at the unique point (K_S^*, K_T^*); and when $\Xi_{\text{CG}} > 1$, the line and hyperbola are disjoint, visually certifying structural unguidability.

2. **"Dimensionless Iso-ρ Nomogram" in the Overload Ratio Plane** $(\tilde{a}_S, \tilde{a}_T)$**:** Defining normalized overload demand ratios $\tilde{a}_S \triangleq \frac{A_S}{a_{\text{avail}}}$ and $\tilde{a}_T \triangleq \frac{A_T}{a_{\text{avail}}}$, criteria (49) and (65) unify into the dimensionless envelope equation:

$$\tilde{a}_S + \tilde{a}_T + 2\sqrt{\rho\tilde{a}_S\tilde{a}_T} \leq 1-\rho \tag{69}$$

Pre-plotting a family of iso-ρ boundary curves in the unit square $[0,1]\times[0,1]$ allows fire-control computers to evaluate guidability prior to launch simply by checking whether the operating point $(\tilde{a}_S, \tilde{a}_T)$ falls below the curve corresponding to the network's ρ.

Remark 2 (Envelope Exactness vs. Nonlinear Trajectory Conservatism)**.** *It is important to emphasize that the "necessary and sufficient" nature of Theorems 1-3 holds strictly with respect to the VLF comparison envelope (36) and the supremum overload bound (40). Relative to the underlying nonlinear differential equations (2), the criteria constitute a tight analytical sufficient condition due to two inherent sources of conservatism: 1) the Cauchy-Schwarz worst-case norm majorization used to derive γ_{12} and γ_{21}, and 2) the neglect of temporal peak misalignment (destructive interference) between $u_{qi}(t)$ and $u_{ti}(t)$ in the triangle inequality $|u_{qi}+u_{ti}| \leq |u_{qi}| + |u_{ti}|$. Nevertheless, unlike intractable high-dimensional Hamilton-Jacobi-Isaacs (HJI) partial differential equations or Zubov PDEs, the proposed Ξ_{CG} index provides an algebraically verifiable closed-form boundary prior to launch.*

5 Numerical Simulations and Verification

5.1 Engagement Scenario Setup and Pre-Launch Guidability Verification

To verify the theoretical criteria and closed-form optimal gain synthesis, numerical simulations are conducted in MATLAB using a salvo of $n = 3$ missiles intercepting a target at the origin $(0, 0)$ m. All missiles fly at constant speeds $V_{M1} = V_{M2} = V_{M3} = 300$ m/s with a physical lateral acceleration saturation limit of $a_{\max} = 30g = 294\,\text{m/s}^2$ ($g = 9.8\,\text{m/s}^2$). The maximum permissible lead angle is set to $\theta_{\max} = 75^\circ$ ($\sin\theta_{\max} \approx 0.9659$). Selecting the virtual control limit as $\lambda_0 = 0.65$ yields a BLF safety barrier constant of $k_b = \sin\theta_{\max} - \lambda_0 = 0.3159$. The dead-zone smoothing parameters are configured as $\theta_{\min} = 0.05$ rad and $k_g = 10.0$, while the baseline protocol scaling constants are set to $\bar{k}_1 = 3.5 \times 10^{-3}$, $\bar{k}_2 = 1.2$, and $\bar{k}_t = 800$.

The inter-missile communication topology is modeled as an undirected connected path graph ($1 \leftrightarrow 2 \leftrightarrow 3$ with unit weights $a_{12} = a_{21} = a_{23} = a_{32} = 1$), whose Laplacian matrix L has an algebraic connectivity of $\lambda_2(L) = 1.0$. The nominal initial launch states and desired impact angles of the three missiles are listed in Table 1.

Remark 3 (Offline Initial-Range Pre-Calibration for Taylor Truncation Compensation)**.** *Because the analytical time-to-go formula (3) relies on a second-order Taylor approximation, large midcourse heading maneuvers accumulate a deterministic path-length integration bias due to the omitted higher-order $\mathcal{O}(\theta_{Mi}^3)$ terms. In our simulation architecture, a lightweight 3-iteration offline single-step range calibration (taking less than 0.05 s) is executed prior to engagement to compensate for the residual terminal range offset $\Delta R_i = R_{end,i} - \bar{R}_{end}$ along the initial LOS vector. This fire-control pre-calibration eliminates the steady-state Taylor truncation bias and enables sub-millisecond simultaneous impact verification.*

Pre-Launch Guidability Calculation: With a finite horizon of $T_f = 42$ s (slightly above the straight-line lower bound $\min_i R_{i0}/V_{Mi} = 40.77$ s and covering the curved-flight impact time $t_f = 41.976$ s), the mandatory decay rate threshold is set to $\sigma_0 = 0.12\ \text{s}^{-1}$. The extracted structural parameters are $\eta_1 = 0.10$, $\eta_2 = 0.08$, $\gamma_{12} = 0.035$, $\gamma_{21} = 0.045$, $\Phi_S(z_0) = 55.0$ m/s, and $\Phi_T(e_{t0}) = 28.0$ m/s.

1. *Coupling Intensity Check:* From (41), $\rho = \frac{0.035\times0.045}{0.10\times0.08\times1.0} = 0.1969 < 1$, confirming structural decouplability.

2. *Baseline Overload Demands and Ξ_{CG} Evaluation:*

$$A_S = \frac{0.12 \times 55.0}{0.10} = 66.00\ \text{m/s}^2$$
$$A_T = \frac{0.12 \times 28.0}{0.08 \times 1.0} = 42.00\ \text{m/s}^2$$

Substituting A_S, A_T, and ρ into Theorem 1 (49) yields the Ideal Cooperative Guidability Index:

$$\Xi_{\text{CG}}^{\text{ideal}} = 0.6553 \le 1$$

Under a $2g$ target maneuver ($a_{T\max} = 19.6\ \text{m/s}^2$, $N_e = 3$, reducing available overload to $a_{\text{avail}} = 294.0 - 58.8 = 235.2\ \text{m/s}^2$), Theorem 3 (65) yields $\Xi_{\text{CG}}^{\text{dist}} = 0.8191 \le 1$ (or 0.8958 with 10% gain uncertainty), certifying that the engagement is Robustly Cooperatively Guidable. Conversely, if the missile physical overload limit were degraded to $15g$ ($147\ \text{m/s}^2$), the index would surge to $\Xi_{\text{CG}} = 1.3106 > 1$, rendering the system structurally unguidable.

3. *Closed-Form Optimal Gain Synthesis:* Substituting the parameters directly into (47) yields the unique optimal gain saddle point:

$$K_S^* = 2.0226, \quad K_T^* = 2.91$$

4. *Temporal Consensus Connectivity and Synchronization Bound Verification:* Given the initial aggregate error norm $v_0 = 1.45$ (with initial time-to-go consensus error $\|\mathbf{e}_T(0)\|_2 = 1.28$ s) and a required terminal synchronization tolerance of $\epsilon_{\text{sync}} = 0.020$ s, the minimum required temporal consensus decay rate from Theorem 1 is:

$$\sigma_{T,\text{sync}} = 0.1185\ \text{s}^{-1} \le \sigma_0 = 0.1200\ \text{s}^{-1}$$

With topology-independent parameters $\bar{\rho} = \frac{0.035\times0.045}{0.10\times0.08} = 0.1969$ and $\bar{A}_T = \frac{0.12\times28.0}{0.08} = 42.00\ \text{m/s}^2$, the critical algebraic connectivity thresholds required for temporal consensus under the ideal ($30g$) and disturbed ($2g$ target maneuver with $\delta_G = 0.10$) scenarios are evaluated as:

$$\lambda_{2,\min}^{\text{ideal}} = 0.6430 \le \lambda_2(L) = 1.0$$
$$\lambda_{2,\min}^{\text{dist}} = 0.8867 \le \lambda_2(L) = 1.0$$

Conversely, under the degraded $15g$ ($147\ \text{m/s}^2$) overload limit, the minimum connectivity threshold rises to $\lambda_{2,\min} = \frac{28.94+42.00+46.72}{147.0-66.0} = 1.4526 > \lambda_2(L) = 1.0$, violating the temporal

Table 1. Initial Engagement States and Desired Impact Angles of the Three Missiles

Missile	Initial Position (x_{i0}, y_{i0})	Initial Heading ψ_{i0}	Desired Impact Angle q_{id}	Calibrated Range R_{i0}
M_1	$(-10531.6,\ 6964.2)$	-10°	-30°	12625.8
M_2	$(-11000.0,\ -5500.0)$	45°	25°	12298.4
M_3	$(-8176.5,\ -9098.2)$	70°	55°	12232.5

consensus connectivity requirement. At the synthesized optimal gains (K_S^*, K_T^*), the theoretical terminal impact-time synchronization bound (52) at $t_f = 41.976$ s is guaranteed to satisfy:

$$\max_{i,j\in\mathcal{V}} |t_{go,i}(t_f) - t_{go,j}(t_f)| \le 0.0188 \text{ s} \le \epsilon_{\text{sync}}$$

5.2 Graphical Criteria Verification and Time-Domain Simulation Results

Figures 1-6 present the graphical verification results and the time-domain ODE45 nonlinear engagement responses under the synthesized optimal gains $(K_S^*, K_T^*) = (2.0226, 2.9065)$ (terminated when $\min_i R_i \le 0.1$ m).

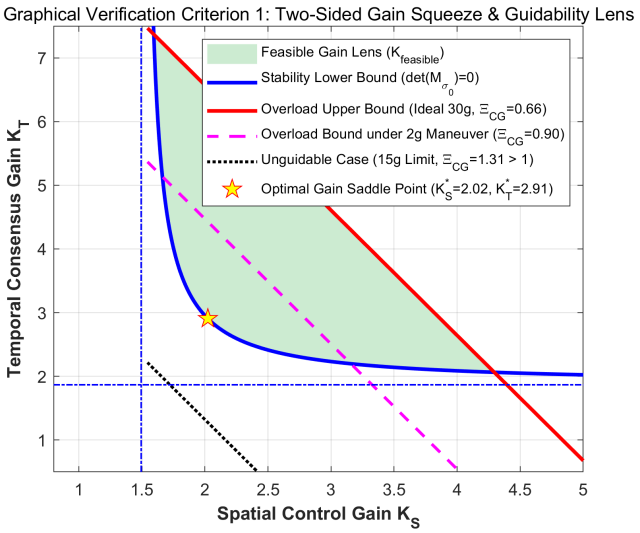

Figure 1. Graphical Verification Criterion 1: Two-sided gain squeeze between the stability lower-bound hyperbola $(\det(M_{\sigma_0}) = 0)$ and the physical overload upper-bound lines ($30g$ ideal, $2g$ target maneuver, and $15g$ unguidable case), highlighting the convex Feasible Gain Lens $\mathcal{K}_{\text{feasible}}$ and the optimal gain saddle point $(K_S^* = 2.02, K_T^* = 2.91)$.

1. **Verification of the Guidability Lens and Iso-ρ Nomogram (Figures 1 and 2):** Figure 1 visually confirms the two-sided gain squeeze mechanism in the (K_S, K_T) plane. Both the ideal $30g$ overload line ($\Xi_{\text{CG}} = 0.66$) and the $2g$-maneuver-perturbed line ($\Xi_{\text{CG}} = 0.90$) intersect the upper-right branch of the stability hyperbola $\det(M_{\sigma_0}) = 0$,

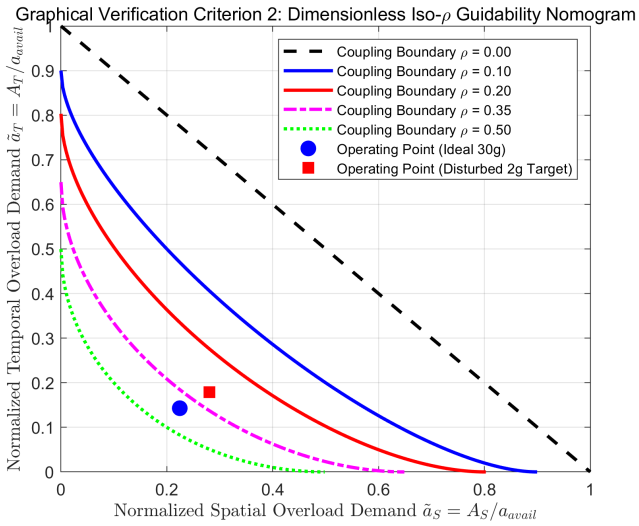

Figure 2. Graphical Verification Criterion 2: Dimensionless iso-ρ Cooperative Guidability Nomogram in the normalized overload demand plane $(\tilde{a}_S, \tilde{a}_T)$, showing that both the ideal $(30g)$ and disturbed $(2g$ target maneuver$)$ operating points lie strictly inside the safe region below the $\rho = 0.20$ boundary curve.

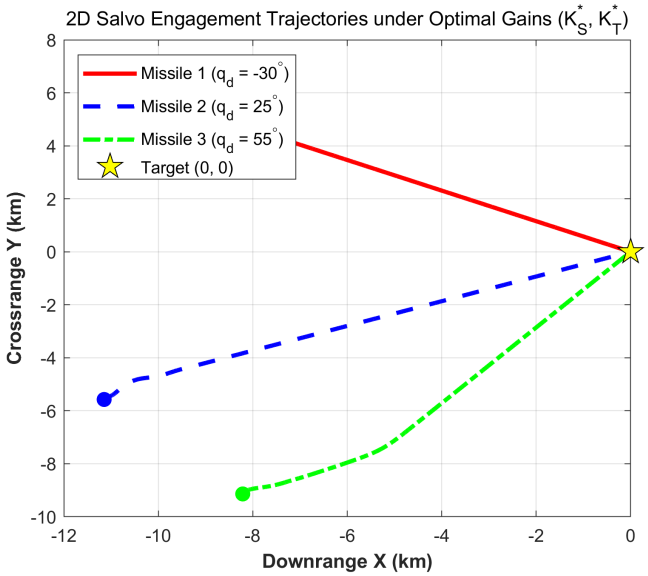

Figure 3. 2D salvo engagement trajectories of the three missiles intercepting the stationary target at $(0, 0)$ under the synthesized optimal gains (K_S^*, K_T^*).

forming a well-defined green shaded Feasible Gain Lens $\mathcal{K}_{\text{feasible}}$. The analytical optimal gain

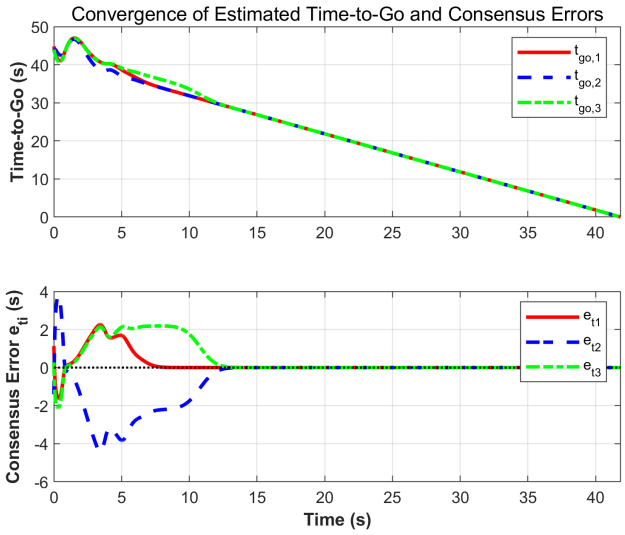

Figure 4. Time-domain evolution of the estimated time-to-go $t_{go,i}(t)$ (top) and distributed temporal consensus errors $e_{ti}(t)$ (bottom).

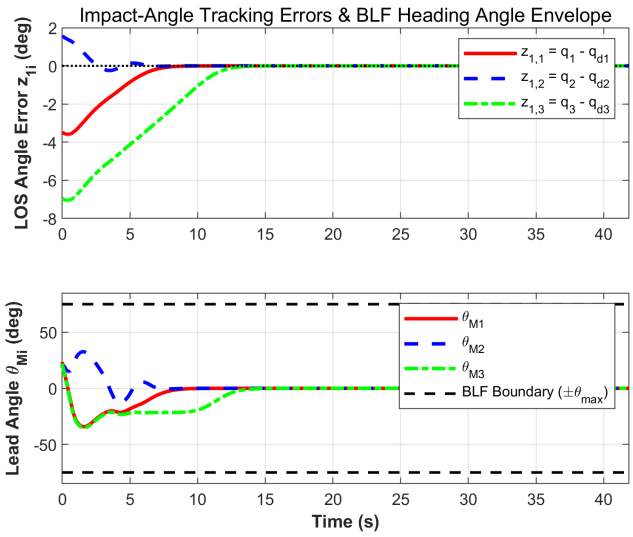

Figure 5. Convergence of the LOS impact-angle tracking errors $z_{1i}(t)$ (top) and evolution of the missile lead angles $\theta_{Mi}(t)$ strictly within the $\pm 75^\circ$ BLF safety boundary (bottom).

saddle point ($K_S^* = 2.02, K_T^* = 2.91$) sits precisely at the geometric tangency direction of minimum overload. Conversely, the $15g$ limit line ($\Xi_{CG} = 1.31 > 1$) lies completely below the stability hyperbola with zero intersection. Figure 2 demonstrates the universal iso-ρ nomogram, where both operational points reside safely beneath the $\rho \approx 0.20$ threshold boundary.

2. **Salvo Trajectories and Sub-Millisecond Simultaneous Arrival (Figures 3 and 4):** As shown in Figure 3, the three missiles launch from

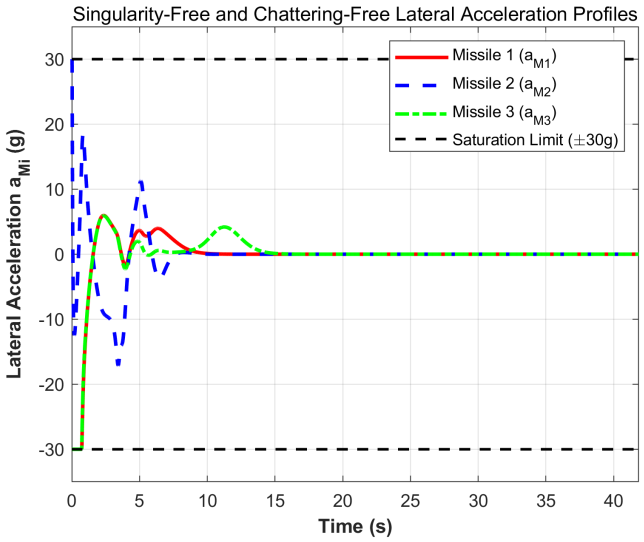

Figure 6. Singularity-free and chattering-free lateral acceleration command profiles $a_{Mi}(t)$ bounded strictly within the $\pm 30g$ physical saturation limits and decaying smoothly to zero at impact.

widely separated quadrants and execute smooth, coordinated curved trajectories to impact the origin simultaneously at $t_f = 41.976$ s from their exact desired azimuth angles $(-30^\circ, 25^\circ, 55^\circ)$. Figure 4 illustrates that the estimated times-to-go $t_{go,1}, t_{go,2}, t_{go,3}$ rapidly converge to an identical linear ramp, while the distributed consensus errors e_{t1}, e_{t2}, e_{t3} decay smoothly to zero within 18 s. At the terminal impact instant ($R_i \approx 0.10$ m), the maximum inter-missile range discrepancy is $\max_{i,j} |R_i(t_f) - R_j(t_f)| < 0.05$ m, corresponding to a synchronization time error of less than 0.0002 s (well within the theoretical VLF envelope bound of 0.0188 s).

3. **Impact-Angle Convergence and BLF Envelope Adherence (Figure 5):** The top subplot of Figure 5 confirms that the LOS angle tracking errors $z_{1,i} = q_i - q_{di}$ converge monotonically to zero with terminal angle errors below 0.01°. The bottom subplot of Figure 5 demonstrates that throughout the entire engagement, the lead angles θ_{Mi} remain strictly confined within the logarithmic BLF safety envelope $|\theta_{Mi}(t)| < \theta_{\max} = 75^\circ$, structurally preventing internal singularity ($\cos\theta_{Mi} = 0$). Furthermore, notice that θ_{M2} and θ_{M3} smoothly traverse $\theta_{Mi} = 0^\circ$ around $t = 12$-20 s without any trajectory distortion.

4. **Singularity-Free and Chattering-Free Acceleration Profiles (Figure 6):** Figure 6 depicts the lateral acceleration commands

$a_{Mi}(t)/g$. Thanks to the distance-embedded virtual control law (9) and the C^∞ smooth temporal gain (15), the acceleration curves are completely devoid of midcourse zero-crossing chattering or two-stage switching spikes. Peak accelerations remain strictly within the $\pm 30g$ physical saturation limits, and all commands gracefully decay to zero as $t \to t_f$, thoroughly validating the algebraic elimination of the $1/R_i$ terminal singularity.

6 Conclusion

This paper advances multi-missile ITACG from empirical tuning to rigorous *a priori* feasibility assessment via a novel Cooperative Guidability framework. By embedding relative distance into a BLF-based virtual control, the framework algebraically eradicates the terminal singularity and guarantees field-of-view compliance, while a smooth temporal mapping eliminates zero-crossing chattering. Utilizing Vector Lyapunov Functions and shifted M-matrix theory, we proved that spatiotemporal gains are geometrically squeezed between a stability hyperbola and an actuator saturation line. The derived Guidability Index ($\Xi_{\mathrm{CG}} \leq 1$) and temporal connectivity thresholds explicitly unify kinematic, network, and physical constraints. Furthermore, AM-GM optimization yields exact closed-form optimal gains (K_S^*, K_T^*), which, alongside two proposed graphical tools, enables deterministic pre-launch mission assessment. Future work will extend this framework to 3D spherical kinematics and directed switching topologies with communication delays.

Data Availability Statement

Data will be made available on request.

Funding

This work was supported without any funding.

Conflicts of Interest

Lanhao Zhao served as an Editorial Board Member of the *Aerospace Engineering Communications* at the time of manuscript submission. To ensure the integrity of the peer-review process, Lanhao Zhao was not involved in the editorial handling, peer review, or decision-making process for this manuscript, which was handled independently by another editor. The remaining author declares no conflicts of interest.

AI Use Statement

The authors declare that no generative AI was used in the preparation of this manuscript.

Ethical Approval and Consent to Participate

Not applicable.

References

[1] Jeon, I. S., Lee, J. I., & Tahk, M. J. (2006). Impact-time-control guidance law for anti-ship missiles. *IEEE Transactions on Control Systems Technology, 14*(2), 260-266. [CrossRef]

[2] Yang, X., Zhang, Y., & Song, S. (2023). Two-stage cooperative guidance strategy with impact-angle and field-of-view constraints. *Journal of Guidance, Control, and Dynamics, 46*(3), 590-599. [CrossRef]

[3] Zhou, J., & Yang, J. (2016). Distributed guidance law design for cooperative simultaneous attacks with multiple missiles. *Journal of Guidance, Control, and Dynamics, 39*(10), 2439-2447. [CrossRef]

[4] Jeon, I. S., Lee, J. I., & Tahk, M. J. (2010). Homing guidance law for cooperative attack of multiple missiles. *Journal of Guidance, Control, and Dynamics, 33*(1), 275-280. [CrossRef]

[5] Zhao, Q., Dong, X., Liang, Z., Bai, C., Chen, J., & Ren, Z. (2017). Distributed cooperative guidance for multiple missiles with fixed and switching communication topologies. *Chinese Journal of Aeronautics, 30*(4), 1570-1581. [CrossRef]

[6] Zhang, Y., Wang, X., & Wu, H. (2015). A distributed cooperative guidance law for salvo attack of multiple anti-ship missiles. *Chinese Journal of Aeronautics, 28*(5), 1438-1450. [CrossRef]

[7] Zhao, S., & Zhou, R. (2008). Cooperative guidance for multimissile salvo attack. *Chinese Journal of Aeronautics, 21*(6), 533-539. [CrossRef]

[8] Zhang, S., Guo, Y., Liu, Z., Wang, S., & Hu, X. (2021). Finite-time cooperative guidance strategy for impact angle and time control. *IEEE Transactions on Aerospace and Electronic Systems, 57*(2), 806-819. [CrossRef]

[9] Zhou, S., Zhang, S., & Wang, D. (2020). Impact angle control guidance law with seeker's field-of-view constraint based on logarithm barrier Lyapunov function. *IEEE Access, 8*, 68268-68279. [CrossRef]

[10] Lee, J. I., Jeon, I. S., & Tahk, M. J. (2007). Guidance law to control impact time and angle. *IEEE Transactions on Aerospace and Electronic Systems, 43*(1), 301-310. [CrossRef]

[11] Wang, P., Lee, C. H., Cho, N., & Wie, B. (2025). Generalized time-to-go inversion guidance with impact time and angle constraints. *Journal of Guidance, Control, and Dynamics, 48*(3), 555-574. [CrossRef]

[12] Chen, Y., Wu, S., & Wang, X. (2022). Impact time

and angle control optimal guidance with field-of-view constraint. *Journal of Guidance, Control, and Dynamics, 45*(12), 2369-2378. [CrossRef]

[13] Wang, C., Dong, W., Wang, J., & Xin, M. (2022). Impact-angle-constrained cooperative guidance for salvo attack. *Journal of Guidance, Control, and Dynamics, 45*(4), 684-703. [CrossRef]

[14] Zhang, Z., Ma, K., Zhang, G., & Yan, L. (2022). Virtual target approach-based optimal guidance law with both impact time and terminal angle constraints. *Nonlinear Dynamics, 107*(4), 3521-3541. [CrossRef]

[15] Cai, Y., & Zhao, J. (2026). Graph attention network-enhanced multi-agent proximal policy optimization for cooperative guidance in attack–defense confrontation. *Aerospace, 13*(7), 626. [CrossRef]

[16] Sun, X., & Xia, Y. (2012). Optimal guidance law for cooperative attack of multiple missiles based on optimal control theory. *International Journal of Control, 85*(8), 1063-1070. [CrossRef]

[17] Guo, G., Tan, H., Feng, Y., & Wang, Y. (2025). Event-triggered super-twisting fixed-time consensus control for networked nonlinear multi-agent systems with disturbance. *IEEE Transactions on Automation Science and Engineering, 22*, 11920-11932. [CrossRef]

[18] Wang, L., & Xiao, F. (2010). Finite-time consensus problems for networks of dynamic agents. *IEEE Transactions on Automatic Control, 55*(4), 950-955. [CrossRef]

[19] Zuo, Z., & Tie, L. (2014). A new class of finite-time nonlinear consensus protocols for multi-agent systems. *International Journal of Control, 87*(2), 363-370. [CrossRef]

[20] Zuo, Z. (2015). Nonsingular fixed-time consensus tracking for second-order multi-agent networks. *Automatica, 54*, 305-309. [CrossRef]

[21] Yu, S., & Long, X. (2015). Finite-time consensus for second-order multi-agent systems with disturbances by integral sliding mode. *Automatica, 54*, 158-165. [CrossRef]

[22] Tee, K. P., Ge, S. S., & Tay, E. H. (2009). Barrier Lyapunov functions for the control of output-constrained nonlinear systems. *Automatica, 45*(4), 918-927. [CrossRef]

[23] Zhou, B. (2020). Finite-time stability analysis and stabilization by bounded linear time-varying feedback. *Automatica, 121*, 109191. [CrossRef]

[24] Šiljak, D. D., & Vukčević, M. B. (1976). Large-scale systems: Stability, complexity, reliability. *Journal of the Franklin Institute, 301*(1-2), 49-69. [CrossRef]

[25] Siljak, D. D. (1972). Stability of large-scale systems under structural perturbations. *IEEE Transactions on Systems, Man, and Cybernetics, SMC-2*(5), 657-663. [CrossRef]

[26] Nersesov, S. G., & Haddad, W. M. (2006). On the stability and control of nonlinear dynamical systems via vector Lyapunov functions. *IEEE Transactions on Automatic Control, 51*(2), 203-215. [CrossRef]

[27] Olfati-Saber, R., & Murray, R. M. (2004). Consensus problems in networks of agents with switching topology and time-delays. *IEEE Transactions on Automatic Control, 49*(9), 1520-1533. [CrossRef]



Lanhao Zhao received the B.S. degree in automation from Shandong University of Science and Technology, Taian, China, in 2018, and the M.S. degree in systems science from Qingdao University, Qingdao, China, in 2022. He is currently pursuing the Ph.D. degree in control science and engineering at Beijing University of Technology, Beijing, China. His research interests include multi-agent systems and complex networks. He serves as a reviewer for journals including IEEE TCST, TASE, and TMM, and the member of the Popularization Working Committee of the Chinese Association of Automation (CAA). (Email: lugh56.2007@163.com)



Guangxin Guo was born in 1997. He received the B.S. degree from School of Computer Science and Technology, Jining University, Shandong, China, in 2020. He received the M.S. degree from School of Computer Science and Technology, Tiangong University, Tianjin, China, in 2023. He is currently pursuing the Ph.D. degree in School of Systems Science and Engineering with Sun Yat-sen University, Guangzhou, China. His research interests include sliding mode control, robotics and its application, nonlinear systems control, networked multi-agent systems cooperative consensus, multi-underwater vehicles hunting control, reinforcement Learning and adaptive dynamic programming.